Measurement of the Deeply Virtual Compton Scattering cross-section off the neutron

M. Mazouz*†, A. Ben Fredj, L. Ghedira

Faculté des Sciences de Monastir, 5000 Monastir, Tunisia

C.E. Hyde†‡, J. Ball, P.-Y. Bertin§, M. Brossard, A. El-Alaoui, A. Fradi, E. Fuchey, M. Garçon, M. Guidal, F. Itard, P. Konczykowski, M. MacCormick, B. Michel, B. Moreno, C. Muñoz Camacho, S. Niccolai, B. Pire, S. Procureur, F. Sabatié, E. Voutier

LPC (Clermont) / LPSC (Grenoble) / IPN (Orsay) / CPhT-Polytechnique (Palaiseau) / SPhN (Saclay) CEA/DSM/DAPNIA & CNRS/IN2P3, France

A. Camsonne†, J.-P. Chen, E. Chudakov, A. Deur, J. Gomez, F.X. Girod, D. Higinbotham, C. W. de Jager, J.J. LeRose, R. Michaels, O. Hansen, A. Saha, S. Stepanyan, V. Sulkolsky, B. Wojtsekhowski

Thomas Jefferson National Accelerator Facility, Newport News, VA 23606, USA

J. Roche, P.M. King

Ohio University, Athens, OH 45701, USA

M. Amarian, M. Canan, G. Gavalian, L.W. Weinstein

Old Dominion University, Norfolk, VA 23529, USA

G.P. Grim, X. Jiang, A. Klein, M.X. Liu

Los Alamos National Laboratory, Los Alamos, NM 87545, USA

P.L. Cole, D.S. Dale, and T.A. Forest

Idaho State University, Pocatello, Idaho 83201, USA

R. De Leo, L. Lagamba, and S. Marrone

* Contact person: mazouz@jlab.org

† co-Spokesperson

‡ and Old Dominion University, Norfolk, VA 23529, USA

§ and Thomas Jefferson National Accelerator Facility, Newport News, VA 23606, USA

Physics Department of Bari University, Italy

E. Cisbani, F. Cusanno, S. Frullani, F. Garibaldi

INFN Roma1 gr. coll. Sanita', Rome, Italy

G. Urcioli

INFN Roma1, Rome, Italy

M. Mihovilovič, M. Potokar, S. Širca

Jožef Stefan Institute and Dept. of Physics, University of Ljubljana, Slovenia

K. Boyle, A. Deshpande, S. Taneja

Stony Brook University, Stony Brook, NY 11794, USA

N. Sparveri

Massachusetts Institute of Technology, Cambridge, MA 02139, USA

Z. Meziani

Temple University, Philadelphia, PA 19122-6082

R. Subedi

Kent State University, Kent, Ohio 44242, USA

H. Benaoum

Syracuse University, Syracuse, New York 13244, USA

and

The Jefferson Lab Hall A Collaboration

We propose to measure the cross section for deeply virtual Compton scattering (DVCS) off the deuteron in quasi-free D$(\vec{e}, e'\gamma)pn$ kinematics at Q^2=1.9 GeV^2 and x_B=0.36. Two incident beam energies (4.82 GeV and 6.0 GeV) will be used in order to separate the interference between DVCS and the Bethe-Heitler (BH) from the pure DVCS^2 contribution. This separation is a necessary step toward an interpretation of the cross section in terms of combinations of generalized parton distribution (GPD) integrals. In the Impulse Approximation, the inelastic DVCS reaction can be interpreted as the incoherent sum of proton and neutron contributions. DVCS on the neutron provide a different flavor sensitivity than DVCS on the proton and is therefore a required step to flavor-separate GPDs. In addition, we will measure the cross sections of DVCS on coherent deuteron (d-DVCS) and the deeply virtual π^0 electroproduction off the neutron. To achieve our goals, we request 400 hours of data taking with Deuterium target during the future p-DVCS experiment (E07-007).

Contents

I. INTRODUCTION AND MOTIVATIONS

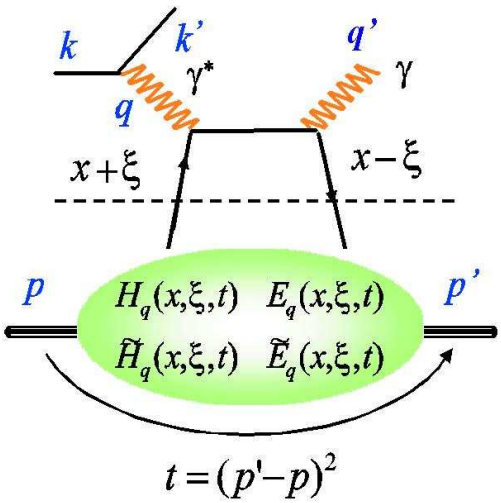

FIG. 1: The handbag diagram for DVCS. An incident lepton of four-momentum k generates a virtual photon of four-momentum $q = k - k'$. The momentum four-vector of the scattered photon is q'. The initial and final momentum four-vectors of the nucleon are p and p' resulting in a total momentum transfer $t = (p' - p)^2 = (q - q')^2$. Additional (e, e') invariants are $y = q \cdot p/(k \cdot p)$, $W^2 = (q + p)^2$, $Q^2 = -q^2$, and $x_B = Q^2/(2q \cdot p)$. The GPD skewness invariant is $\xi = x_B/(2 - x_B)$.

Generalized parton distributions (GPDs) are a new theoretical tool, developed in the late 90s, which link form factors and parton distributions. They offer correlation information between the transverse location and the longitudinal momentum of partons and can access the contribution of the orbital angular momentum of quarks (and gluons) to the nucleon spin [1–3]. Deeply Virtual Compton Scattering (DVCS) on the nucleon is the simplest hard exclusive process involving GPDs, and have simulated an intense experimental effort. The H1 [4, 5] and ZEUS [6] collaborations measured the cross section for $x_{\rm Bj} \approx 10^{-3}$. The HERMES collaboration measured relative beam-helicity [7] and beam-charge asymmetries [8, 9]. Relative beam-helicity [10, 11] and longitudinal target [12] asymmetries were measured at JLab by the CLAS collaboration. Cross-sections measurements on the proton in the valence quark region by the Hall-A collaboration at JLab showed indications of twist-2 dominance at $Q^2 \approx 2$ GeV^2 [13].

Fig. 1 shows the leading twist mechanism for DVCS. A virtual photon scatters on a single quark with a given longitudinal momentum fraction $x+\xi$. This quark becomes highly virtual and re-emits a real photon before coming back into the nucleon with a different longitudinal momentum $x - \xi$. The amplitude to remove and restore the parton inside the nucleon is

described, at the leading order in $1/Q$, in terms of four GPDs H, $\tilde{H}$, E and $\tilde{E}$ depending on the three variables x, ξ and the momentum transfer t. The GPDs appear in the DVCS amplitude under integrals over the variable x:

$$\mathcal{T}_{DVCS} \propto \int_{-1}^{1} dx \left(\frac{1}{x-\xi+i\epsilon} \pm \frac{1}{x+\xi-i\epsilon} \right) GPD(x,\xi,t)\,, \tag{1}$$
$$\propto P\int_{-1}^{1} dx \left(\frac{1}{x-\xi} \pm \frac{1}{x+\xi} \right) GPD(x,\xi,t) \; - i\pi \Big[GPD(\xi,\xi,t) \pm GPD(-\xi,\xi,t) \Big]\,.$$

Experimentally DVCS interferes with the Bethe-Heitler (BH) process where the real photon is radiated by the incident or the scattered lepton (see Fig. 2). In Hall A at Jefferson Lab, we measure both the polarized cross section difference with longitudinally polarized electrons and the unpolarized cross section. At leading twist:

$$\overrightarrow{\sigma} - \overleftarrow{\sigma} \sim 2 \cdot \Im m(\mathcal{T}^{BH} \cdot \mathcal{T}^{DVCS})\,, \tag{2}$$
$$\overrightarrow{\sigma} + \overleftarrow{\sigma} \sim \left|\mathcal{T}^{BH}\right|^2 + 2 \cdot \Re e(\mathcal{T}^{BH} \cdot \mathcal{T}^{DVCS}) + \left|\mathcal{T}^{DVCS}\right|^2. \tag{3}$$

Since the BH is purely real and fully calculable with the known form factors, the polarized cross section difference accesses the imaginary part of the DVCS amplitude and therefore a linear combination of GPDs at one point $x = \pm\xi$, while the unpolarized cross section accesses the real part of DVCS and therefore a linear combinations of GPD integrals over x (see Eq. 1). In addition, the unpolarized cross section allows to access the $\left|\mathcal{T}^{DVCS}\right|^2$ term which represents a bilinear combination of GPD integrals.

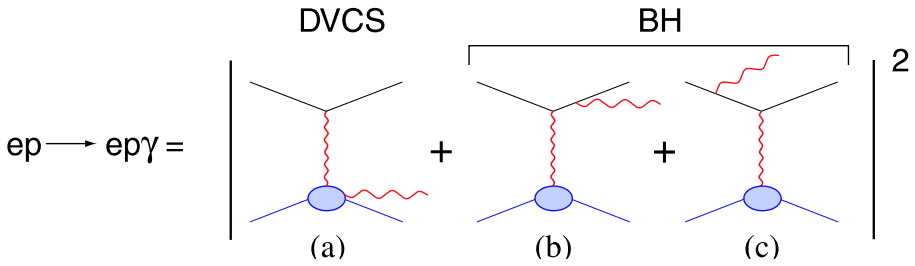

FIG. 2: Lowest order QED diagrams for the process $eN \to eN\gamma$, including the DVCS (a) and the Bethe-Heitler (b, c) amplitudes.

To investigate neutron structure via electron scattering, a deuterium target frequently serves as a quasi-free neutron target because of the weak binding energy between the proton and the neutron inside the deuteron. Within the impulse approximation (IA), where only one nucleon is active and participates in the absorption and emission of the photon (the other

nucleon being a spectator), the electroproduction of photons on a deuterium target may be decomposed into elastic (d-DVCS) and quasi-elastic (p-DVCS and n-DVCS) contributions:

$$\mathrm{D}(\vec{e},e'\gamma)X = d(\vec{e},e'\gamma)d + n(\vec{e},e'\gamma)n + p(\vec{e},e'\gamma)p + \ldots \quad (4)$$

Meson production channels also contribute as background at large M_X^2. Therefore, with a deuterium target one can have three different DVCS processes: DVCS on the nucleon (p-DVCS and n-DVCS) and coherent DVCS on the deuteron (d-DVCS), which accesses deuteron GPDs [14–17]. Cross sections of n-DVCS (and d-DVCS) are then obtained from $\mathrm{D}(\vec{e},e'\gamma)X$ events after subtraction of the proton quasi-elastic contribution deduced from measurements on a H_2 target.

Two experiments, dedicated respectively to p-DVCS and n-DVCS, ran in fall 2004 in Hall A. The p-DVCS experiment (E00-110) showed strong evidence of DVCS scaling for Q^2 as low as 2 GeV^2 [13]. This is a necessary step before interpreting the polarized cross-sections in terms of GPDs. We measured the first linear combinations of proton GPDs at three different Q^2 and at fixed x_B. These combinations are mainly sensitive to H and $\tilde{H}$. In the n-DVCS experiment (E03-106) we extracted, from the helicity-dependent cross section of $\mathrm{D}(\vec{e},e'\gamma)X$ reaction on quasi-free neutrons off deuterium target, the same linear combination of GPDs, but with different weights (a consequence of the different neutron BH amplitude). The neutron helicity dependent cross section was mostly sensitive to $E(\pm\xi,\xi,t)$, the least constrained GPD [18]. The knowledge of E is essential because it enters on equal footing with H in Ji's sum rule leading to the total angular momentum carried by quarks in the nucleon [3]. In addition to providing different GPDs combinations, the neutron experiments have naturally a different flavor sensitivity to GPDs than the proton experiments and they appear as a mandatory step toward a better knowledge of the partonic structure of the nucleon. Figure 3 is a beautiful illustration of this complementarity between the neutron and the proton experiments.

Measurements of the unpolarized cross section are of great interest since they can access GPD integrals over x and therefore explore the regions $|x| \neq \xi$. Unfortunately, these measurements could not be done in E03-106. On the one hand, the interpretation of the unpolarized cross section in terms of GPD integrals requires the knowledge of the $\left|\mathcal{T}^{DVCS}\right|^2$ term in Eq. 3. Both the E00-110 results and theoretical model calculations suggest that this term cannot be neglected. A simultaneous extraction of a linear combination of GPDs

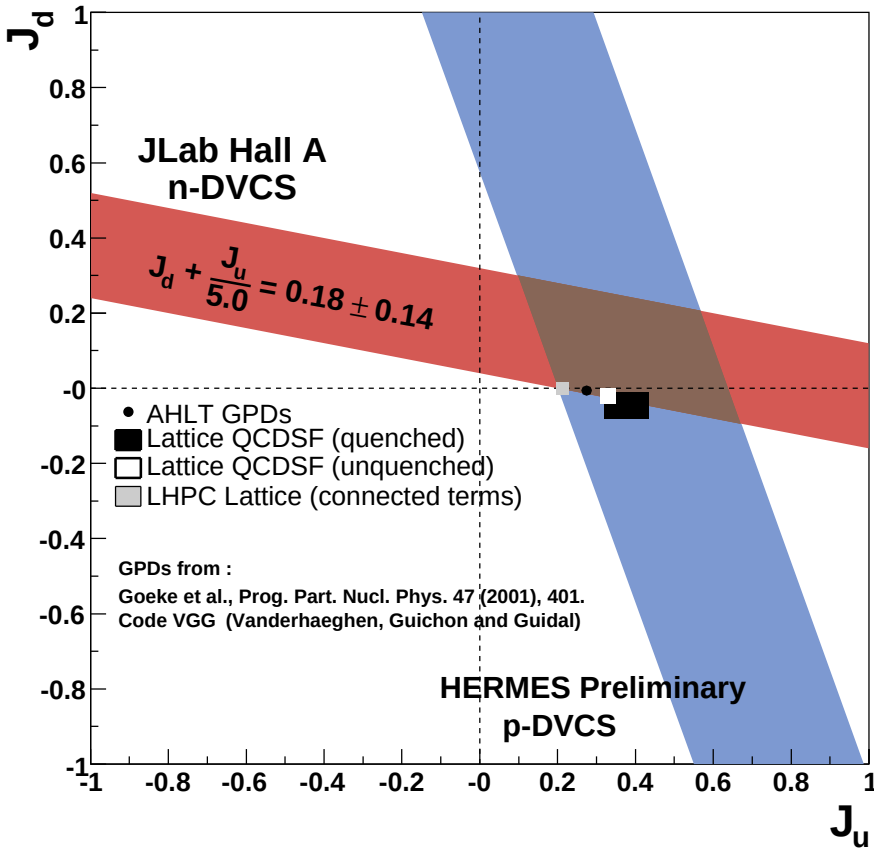

FIG. 3: A model-dependent extraction of the contributions J_u and J_d of up- and down-quarks, respectively to the proton spin [18].

integral (interference term) and a bilinear combination of GPDs (DVCS^2 term), through the unpolarized cross section, requires data with two different beam energies, which was not performed in E03-106. On the other hand, our measurement of the unpolarized cross section in E03-106 had very large systematic error bars ($\sim$50%). The latter is the consequence of:

- A large systematic error due to the uncertainty on the relative calibration between the H_2 and the D_2 data (almost one month separated the two data taking periods).
- A large systematic error due to the contamination of the DVCS-like channel $eD \rightarrow e'\pi^0 X \rightarrow e'\gamma X$. In fact, a high trigger threshold did not allow the recording of enough π^0 decays to properly evaluate this contamination.

We propose in this experiment to accurately measure the DVCS unpolarized cross-section off the neutron at Q^2=1.9 GeV^2 and x_B=0.36. We request 400 hours of beam time with a 15 cm liquid D_2 target at 4.82 GeV (200 h) and 6.0 GeV (200 h) in order to separate the DVCS^2 and the interference contributions

and therefore extract linear and bilinear combinations of GPD integrals. These combinations have naturally a different flavor sensitivity than the ones extracted from proton experiments. We will use exactly the same successful technique from the previous n-DVCS experiment where we detected only the scattered electron (in the HRS-L spectrometer) and the emitted photon (in a PbF_2 calorimeter). The DVCS events are then identified with the missing mass technique and the n-DVCS (and d-DVCS) contribution is obtained, within the impulse approximation, by subtracting the H_2 data from the D_2 data. It should be noticed that 120 hours of H_2 data taking at the proposed kinematics are already approved for the future p-DVCS experiment (E07-007) [19]. The requested beam time is adjusted to have approximately the same statistics for D_2 and H_2 data. The experimental apparatus will be the one used in the two previous DVCS experiments in Hall A with some modifications and upgrades already planned for E07-007. The contamination of the π^0 electroproduction channel will be precisely evaluated with a new global-sum digital trigger on the calorimeter. This will provide a larger acceptance for $\mathrm{D}(e, e'\gamma\gamma)X$ events, and will thereby remove the systematic error due to this contamination. Finally, the problem of the uncertainty on the relative calibration of the calorimeter will be removed by alternating frequently between H_2 and D_2 data taking. We expect, based on the previous DVCS experiments and these improvements, 5% systematic errors on the cross section measurements.

The proposed experiment will provide in addition :

- Polarized cross sections of the π^0 electroproduction off an unpolarized deuterium target, including a L/T separation. The comparison of these results to the proton is very interesting regarding factorization in the $eN \to e'\pi^0 N$ channel and will constrain parton and GPDs models.

- Polarized coherent DVCS cross-sections of the deuteron. The same azimuthal and incident energy analysis will be performed to extract the different harmonic contributions to the cross-section. This will provide unique constraints on deuteron GPDs.

- Measurement of the n-DVCS helicity dependent cross section and the corresponding linear combination of GPDs (at $x = \pm\xi$) with a factor 2 improvement on the total error bars with respect to E03-106.

II. DEEP PHOTON ELECTROPRODUCTION ON THE NEUTRON

As shown in Fig. 2, both DVCS and BH processes contribute to the photon electroproduction cross section. In the differential phase space element $d^5\Phi = dQ^2 dx_{\rm B} dt d\phi_e d\phi_{\gamma\gamma}$, where ϕ_e is the azimuthal angle of the scattered electron and $\phi_{\gamma\gamma}$ is the angle between the leptonic and hadronic planes, the total cross section of photon electroproduction off an unpolarized target of mass M is given by [20]:

$$\begin{aligned}\frac{d^5\sigma(\lambda,\pm e)}{d^5\Phi} &= \frac{d\sigma_0}{dQ^2 dx_B}\left|\mathcal{T}^{BH} \pm \mathcal{T}^{DVCS}(\lambda)\right|^2 \frac{1}{e^6} \\ &= \frac{\alpha^3_{QED} x_B y^2}{16\pi^2 Q^4\sqrt{1+\epsilon^2_{DVCS}}}\left[\left|\mathcal{T}^{BH}\right|^2 + \left|\mathcal{T}^{DVCS}(\lambda)\right|^2 \mp \mathcal{I}(\lambda)\right]\frac{1}{e^6}, \end{aligned} \tag{5}$$

where $\epsilon_{DVCS} = 2x_B M/Q$, λ is the electron helicity and the $\pm$ stands for the sign of the charge of the lepton beam. Since the BH contribution is completely calculable in QED from the well known form factors at small $|t|$, a measurement of the polarized cross section will access the interference ($\mathcal{I}$) and the DVCS^2 ($\left|\mathcal{T}^{DVCS}\right|^2$) terms which depend respectively on a linear and a bilinear combination of GPD integrals. It is possible then to perform a $\phi_{\gamma\gamma}$ analysis in order to separate up to a certain degree the different contributions to the cross sections. At twist-3 accuracy [20]:

$$\mathcal{I}(\lambda) = \frac{e^6}{x_B y^3 \mathcal{P}_1(\phi_{\gamma\gamma})\mathcal{P}_2(\phi_{\gamma\gamma}) t}\left\{c_0^{\mathcal{I}} + \sum_{n=1}^{2}(-1)^n\left[c_n^{\mathcal{I}}(\lambda)\cos(n\phi_{\gamma\gamma}) - \lambda s_n^{\mathcal{I}}\sin(n\phi_{\gamma\gamma})\right]\right\} \tag{6}$$

$$\left|\mathcal{T}^{DVCS}(\lambda)\right|^2 = \frac{e^6}{y^2 Q^2}\left\{c_0^{DVCS} - c_1^{DVCS}\cos(\phi_{\gamma\gamma}) + \lambda s_1^{DVCS}\sin(\phi_{\gamma\gamma})\right\}. \tag{7}$$

$\mathcal{P}_{1,2}$ are the electron propagators of the BH amplitude with a $\phi_{\gamma\gamma}$ dependence. In the previous equations, only the $\sin(n\phi_{\gamma\gamma})$ terms depend of the electron helicity. Consequently, the unpolarized cross section has a $\cos(n\phi_{\gamma\gamma})$ harmonic structure and the helicity-dependent cross section has a $\sin(n\phi_{\gamma\gamma})$ harmonic structure. It should be noticed that we have neglected the gluon tansversity terms, having a $\cos(3\phi_{\gamma\gamma})$ weighting in Eq. 6 and a $\cos(2\phi_{\gamma\gamma})$ weighting in Eq. 7, because our measurements are in the valence quark region (x_B=0.36).

A. Interference Terms

The Fourier coefficients $c_n^{\mathcal{I}}$ and $s_n^{\mathcal{I}}$ of the interference term (Eq. 6) are:

$$\begin{aligned}
c_0^{\mathcal{I}} &= -8(2-y)\Re\mathrm{e}\left\{\frac{(2-y)^2}{1-y}K^2\mathcal{C}^{\mathcal{I}}(\mathcal{F}) + \frac{t}{Q^2}(1-y)(1-x_B)\left[\mathcal{C}^{\mathcal{I}}+\Delta\mathcal{C}^{\mathcal{I}}\right](\mathcal{F})\right\} \\
\begin{Bmatrix} c_1^{\mathcal{I}} \\ s_1^{\mathcal{I}} \end{Bmatrix} &= -8K\begin{Bmatrix} (2-2y+y^2) \\ -y(2-y) \end{Bmatrix}\begin{Bmatrix} \Re\mathrm{e} \\ \Im\mathrm{m} \end{Bmatrix}\mathcal{C}^{\mathcal{I}}(\mathcal{F}) \\
\begin{Bmatrix} c_2^{\mathcal{I}} \\ s_2^{\mathcal{I}} \end{Bmatrix} &= \frac{-16K^2}{2-x_B}\begin{Bmatrix} (2-y) \\ -y \end{Bmatrix}\begin{Bmatrix} \Re\mathrm{e} \\ \Im\mathrm{m} \end{Bmatrix}\mathcal{C}^{\mathcal{I}}(\mathcal{F}^{\mathrm{eff}}),
\end{aligned} \tag{8}$$

where at the Bjorken limit

$$K^2 = \frac{t_{\min}-t}{Q^2}\left[1-x_B\right]\left[1-y\right]\left[1+\mathcal{O}(t/Q^2)\right]\ . \tag{9}$$

The $\mathcal{C}^{\mathcal{I}}$ and $\Delta\mathcal{C}^{\mathcal{I}}$ are the quantities to be extracted from the data and depend on the interference of the BH amplitude with the set $\mathcal{F} = \{\mathcal{H}, \mathcal{E}, \tilde{\mathcal{H}}\}$ of twist-2 Compton form factors (CFFs) or the related set $\mathcal{F}^{\mathrm{eff}}$ of effective twist-3 CFFs:

$$\mathcal{C}^I(\mathcal{F}) = F_1(t)\mathcal{H}(\xi,t) + \xi G_M(t)\tilde{\mathcal{H}}(\xi,t) - \frac{t}{4M^2}F_2(t)\mathcal{E}(\xi,t) \tag{10}$$

$$\mathcal{C}^I(\mathcal{F}^{\mathrm{eff}}) = F_1(t)\mathcal{H}^{\mathrm{eff}}(\xi,t) + \xi G_M(t)\tilde{\mathcal{H}}^{\mathrm{eff}}(\xi,t) - \frac{t}{4M^2}F_2(t)\mathcal{E}^{\mathrm{eff}}(\xi,t) \tag{11}$$

$$\left[\mathcal{C}^I+\Delta\mathcal{C}^I\right](\mathcal{F}) = F_1(t)\mathcal{H}(\xi,t) - \frac{t}{4M^2}F_2(t)\mathcal{E}(\xi,t) - \xi^2 G_M(t)\left[\mathcal{H}(\xi,t)+\mathcal{E}(\xi,t)\right]\ , \tag{12}$$

where F_1 and F_2 are respectively the Dirac and Pauli form factors and $G_M = F_1 + F_2$. As mentioned above, $\mathcal{C}^{\mathcal{I}}(\mathcal{F}^{\mathrm{eff}})$ is a twist-3 term and has a $\sin(2\phi_{\gamma\gamma})$ or $\cos(2\phi_{\gamma\gamma})$ weighting. E00-110 results indicate that the contribution of this term to the polarized cross sections is small relatively to the twist-2 terms [13]. Therefore in E03-106, we have neglected the contribution of this term in our analysis. However, it would be exciting if it could generate a measurable signal.

The imaginary part of twist-2 CFFs is determined by the $x = \pm\xi$ points of the GPDs, whereas the real part is determined by a GPD integral over x. For example:

$$\mathcal{E}(\xi,t) = \sum_f e_f^2\left\{i\pi\Big[E_f(\xi,\xi,t) - E_f(-\xi,\xi,t)\Big] + \mathcal{P}\int_{-1}^{+1}dx\left[\frac{2x}{\xi^2-x^2}\right]E_f(x,\xi,t)\right\} \tag{13}$$

$$\tilde{\mathcal{E}}(\xi,t) = \sum_f e_f^2\left\{i\pi\Big[\tilde{E}_f(\xi,\xi,t) + \tilde{E}_f(-\xi,\xi,t)\Big] + \mathcal{P}\int_{-1}^{+1}dx\left[\frac{2\xi}{\xi^2-x^2}\right]\tilde{E}_f(x,\xi,t)\right\}, \tag{14}$$

where the sum $f \in \{u,d,s\}$ runs over the flavor content of the nucleon, and e_f is the quark charge in unit of the elementary charge. From the previous equations, we can deduce that a

measurement of the unpolarized cross section accesses the real part of CFFs and therefore a GPD integral over x, while a measurement of the helicity-dependent cross section probes the imaginary part of CFFs and therefore GPDs at $x = \pm\xi$.

B. DVCS^2 Terms

The bilinear DVCS Fourier coefficients are:

$$\begin{aligned} c_0^{DVCS} &= 2(2-2y+y^2)\mathcal{C}^{DVCS}(\mathcal{F},\mathcal{F}^*) \\ \begin{Bmatrix} c_1^{DVCS} \\ s_1^{DVCS} \end{Bmatrix} &= \frac{8K}{2-x_B} \begin{Bmatrix} 2-y \\ -y \end{Bmatrix} \begin{Bmatrix} \Re\mathrm{e} \\ \Im\mathrm{m} \end{Bmatrix} \mathcal{C}^{DVCS}(\mathcal{F}^{eff},\mathcal{F}^*)\,. \end{aligned} \tag{15}$$

$\mathcal{C}^{DVCS}(\mathcal{F},\mathcal{F}^*)$ is the only twist-2 DVCS angular harmonic term. It is a bilinear combination of CFFs:

$$\begin{aligned} \mathcal{C}^{DVCS}(\mathcal{F},\mathcal{F}^*) = \frac{1}{(2-x_B)^2}\Big\{ & 4(1-x_B)\left(\mathcal{H}\mathcal{H}^* + \tilde{\mathcal{H}}\tilde{\mathcal{H}}^*\right) - x_B^2 2\Re\mathrm{e}\left[\mathcal{H}\mathcal{E}^* + \tilde{\mathcal{H}}\tilde{\mathcal{E}}^*\right] \\ & - \left(x_B^2 + (2-x_B)^2\frac{t}{4M^2}\right)\mathcal{E}\mathcal{E}^* - x_B^2\frac{t}{4M^2}\tilde{\mathcal{E}}\tilde{\mathcal{E}}^*\Big\}\,. \end{aligned} \tag{16}$$

The twist-3 term $\mathcal{C}^{DVCS}(\mathcal{F}^{\mathrm{eff}},\mathcal{F}^*)$ has an identical form, with the CFFs $\mathcal{F}$ replaced by the set $\mathcal{F}^{\mathrm{eff}}$. Again, the measurement of the twist-3 terms is not among our proposal goals. However, it will be possible to put an experimental upper limit to these contributions in this new experiment.

C. Separation of the Interference and the DVCS^2 Terms

Let us summarize the equations of the previous sections. If we neglect all twist-3 and gluon terms, the DVCS helicity-independent ($d\sigma$) and helicity-dependent ($d\Sigma$) cross sections read

$$\begin{aligned} \frac{d^5\sigma}{d^5\Phi} &= \frac{1}{2}\left[\frac{d^5\sigma^+}{d^5\Phi} + \frac{d^5\sigma^-}{d^5\Phi}\right] = \frac{d^5\sigma(|BH|^2)}{d^5\Phi} + \Gamma_{DVCS}\,\mathcal{C}^{DVCS}(\mathcal{F},\mathcal{F}^*) \\ &+ \frac{1}{\mathcal{P}_1(\phi_{\gamma\gamma})\mathcal{P}_2(\phi_{\gamma\gamma})}\left(\{\Gamma_0^{\Re} - \cos(\phi_{\gamma\gamma})\Gamma_1^{\Re}\}\Re\mathrm{e}\left[\mathcal{C}^I(\mathcal{F})\right] + \Gamma_{0,\Delta}^{\Re}\Re\mathrm{e}\left[\mathcal{C}^I + \Delta\mathcal{C}^I\right](\mathcal{F})\right) \end{aligned} \tag{17}$$

$$\frac{d^5\Sigma}{d^5\Phi} = \frac{1}{2}\left[\frac{d^5\sigma^+}{d^5\Phi} - \frac{d^5\sigma^-}{d^5\Phi}\right] = \frac{1}{\mathcal{P}_1(\phi_{\gamma\gamma})\mathcal{P}_2(\phi_{\gamma\gamma})}\left(\sin(\phi_{\gamma\gamma})\Gamma_1^{\Im}\,\Im\mathrm{m}\left[\mathcal{C}^I(\mathcal{F})\right]\right), \tag{18}$$

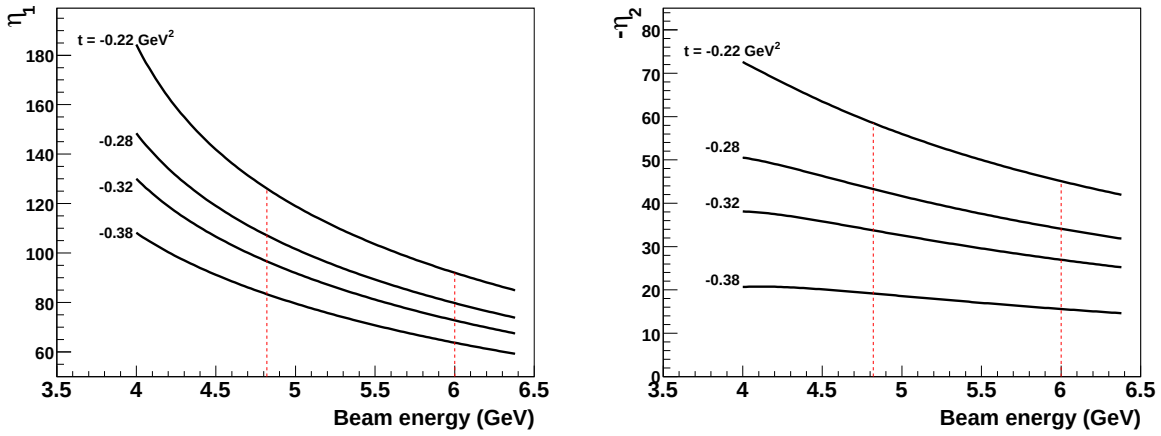

FIG. 4: η_1 (left) and $-\eta_2$ (right) as functions of the beam energy for different values of t at $Q^2 = 1.9$ GeV^2 and x_B=0.36. These variables are defined in Eqs. 22, 23. The dashed lines show the two requested beam energies.

where $\Gamma^{\Re,\Im}$ are kinematical factors with no $\phi_{\gamma\gamma}$ dependence [20]. The harmonic $\phi_{\gamma\gamma}$ structure of the DVCS cross section does *not* allow the independent determination of $\Re\mathrm{e}\left[\mathcal{C}^I\right]$, $\Re\mathrm{e}\left[\mathcal{C}^I + \Delta\mathcal{C}^I\right]$ and $\mathcal{C}^{DVCS}$. Indeed, the interference $\mathcal{I}$ and DVCS^2 terms have the following harmonic structure (with $Q = \sqrt{Q^2}$):

$$\begin{aligned} \mathcal{I} &= \frac{i_0/Q^2 + i_1\cos\varphi/Q + i_2\cos 2\varphi/Q^2 + i_3\cos 3\varphi/Q}{\mathcal{P}_1\mathcal{P}_2} \\ \mathrm{DVCS}^2 &= d_0/Q^2 + d_1\cos\varphi/Q^3 + d_2\cos 2\varphi/Q^4\,. \end{aligned} \tag{19}$$

The product of the BH propagators reads:

$$\mathcal{P}_1\mathcal{P}_2 = 1 + \frac{p_1}{Q}\cos\varphi + \frac{p_2}{Q^2}\cos 2\varphi\,. \tag{20}$$

Reducing to a common denominator ($\times\mathcal{P}_1\mathcal{P}_2$), one obtains:

$$\begin{aligned} \mathcal{P}_1\mathcal{P}_2\mathcal{I} + \mathcal{P}_1\mathcal{P}_2\mathrm{DVCS}^2 &= \boxed{(i_0 + d_0)/Q^2} + d_1p_1/2/Q^4 + p_2d_2/2/Q^6 \\ &+ [i_1/Q + (p_1d_0 + d_1)/Q^3 + (p_1d_2 + p_2d_1)/2/Q^5]\cos\varphi \\ &+ [i_2/Q^2 + (p_2d_0 + p_1d_1/2 + d_2)/Q^4]\cos 2\varphi \\ &+ [i_3/Q + (p_1d_2 + p_2d_1)/2/Q^5]\cos 3\varphi \\ &+ [p_2d_2/4/Q^6]\cos 4\varphi\,. \end{aligned} \tag{21}$$

One sees in Eq. 21 that the interference $\mathcal{I}$ and the DVCS^2 terms **mix at leading order in 1/Q** in the azimuthal expansion.

In order to separate the interference and the DVCS^2 contributions, we have to measure accurately the cross section at constant x_B, t and Q^2 but at two different incident beam energies. That is possible thanks to the sufficiently different dependence on the beam energy of the DVCS^2 and Interference kinematic coefficients of Eq. 17. It should be noted that this separation technique will also be performed in the future proton experiment E07-007 [19]. Figure 4 shows the ratios

$$\eta_1 = \int_{\phi_{\gamma\gamma}} \frac{1}{\mathcal{P}_1(\phi_{\gamma\gamma})\mathcal{P}_2(\phi_{\gamma\gamma})} \Gamma^{\Re}_{0,\Delta} / \Gamma_{DVCS} \tag{22}$$

$$\eta_2 = \int_{\phi_{\gamma\gamma}} \frac{1}{\mathcal{P}_1(\phi_{\gamma\gamma})\mathcal{P}_2(\phi_{\gamma\gamma})} \left(\Gamma^{\Re}_0 - \cos(\phi_{\gamma\gamma})\Gamma^{\Re}_1\right) / \Gamma_{DVCS} \tag{23}$$

as functions of the beam energy and for different values of t. One should notice that $\mathcal{C}^{DVCS}$ is, in average, kinematically suppressed by at least a factor 10 relative to $\Re\mathrm{e}\left[\mathcal{C}^I\right]$ and $\Re\mathrm{e}\left[\mathcal{C}^I + \Delta\mathcal{C}^I\right]$. However its contribution to the cross section might be important due to a large value of the $\mathcal{C}^{DVCS}$ term as suggested by E00-110 results and model calculations based on GPDs (cf. the following section).

D. Neutron GPD Model Estimates

Figure 5 shows an estimate with the VGG model [21, 22] of the GPD combinations that will be extracted from the data. According to this model, the $\mathcal{C}^{DVCS}$ term is roughly 100 times larger than the interference terms $\Re\mathrm{e}\left[\mathcal{C}^I\right]$ and $\Re\mathrm{e}\left[\mathcal{C}^I + \Delta\mathcal{C}^I\right]$. Indeed, in the $\mathcal{C}^{DVCS}$ term, there are no neutron form factors weighting the GPDs (Eq. 15), as in the interference terms (Eqs. 10- 12). Therefore there is no reason to expect a small value for the $\mathcal{C}^{DVCS}$ term. Figure 5 shows also that roughly 30% of the $\mathcal{C}^{DVCS}$ value comes from the GPD $\widetilde{E}$ contribution. This means our future neutron measurements will contribute to constrain the parametrization of the unknown GPD $\widetilde{E}$. Figure 6 shows the expected cross section of photon electroproduction off the neutron (Eq. 17 integrated over ϕ_e) for the two requested beam energies, as well as the different contributions to the cross section. According to the VGG model, the BH^2 and DVCS^2 terms together dominate the cross sections. If we subtract the known BH^2 from the cross section we will measure essentially the DVCS^2 contribution. The beam energy dependence of the DVCS^2/BH^2 ratio is again the key for the separation of the DVCS^2 and interference terms.

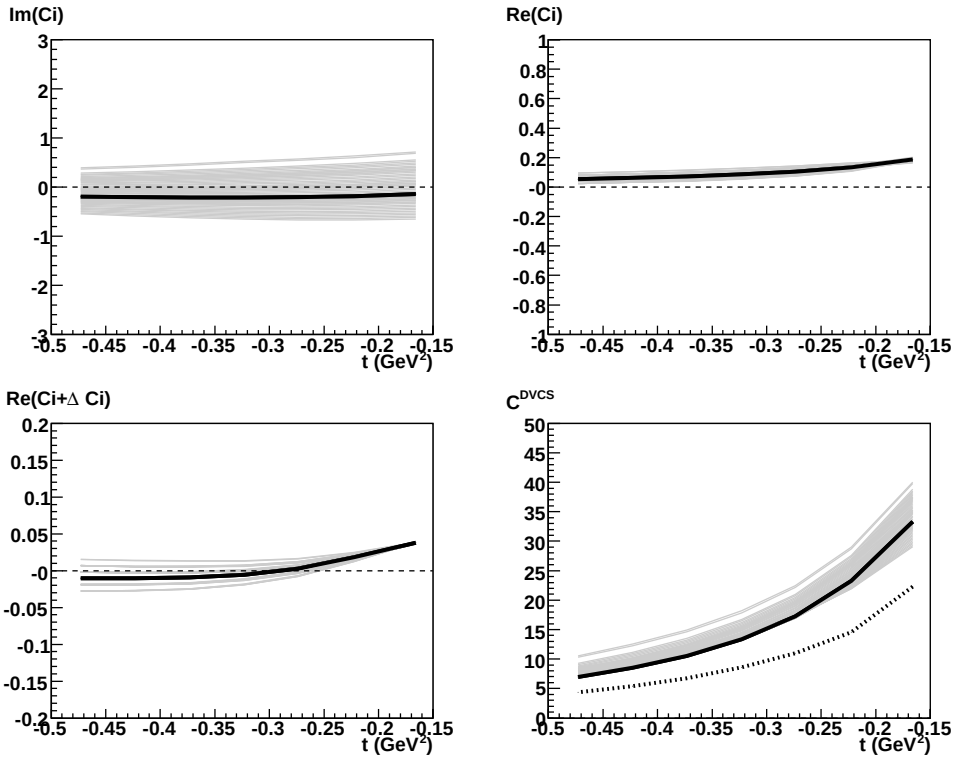

FIG. 5: VGG calculation of the neutron observables to be extracted from the data at our kinematics and as function of t. The GPD E is parametrized by the quark angular momenta J_u and J_d; the bands illustrate the possible values of the observables within the J_u and J_d range determined in E03-106 [18]. Solid lines correspond to $J_u = 0.3$ and J_d=0.2. The dashed curve in the fourth plot represents the $\mathcal{C}^{DVCS}$ values calculated without the GPD $\widetilde{E}$ contribution.

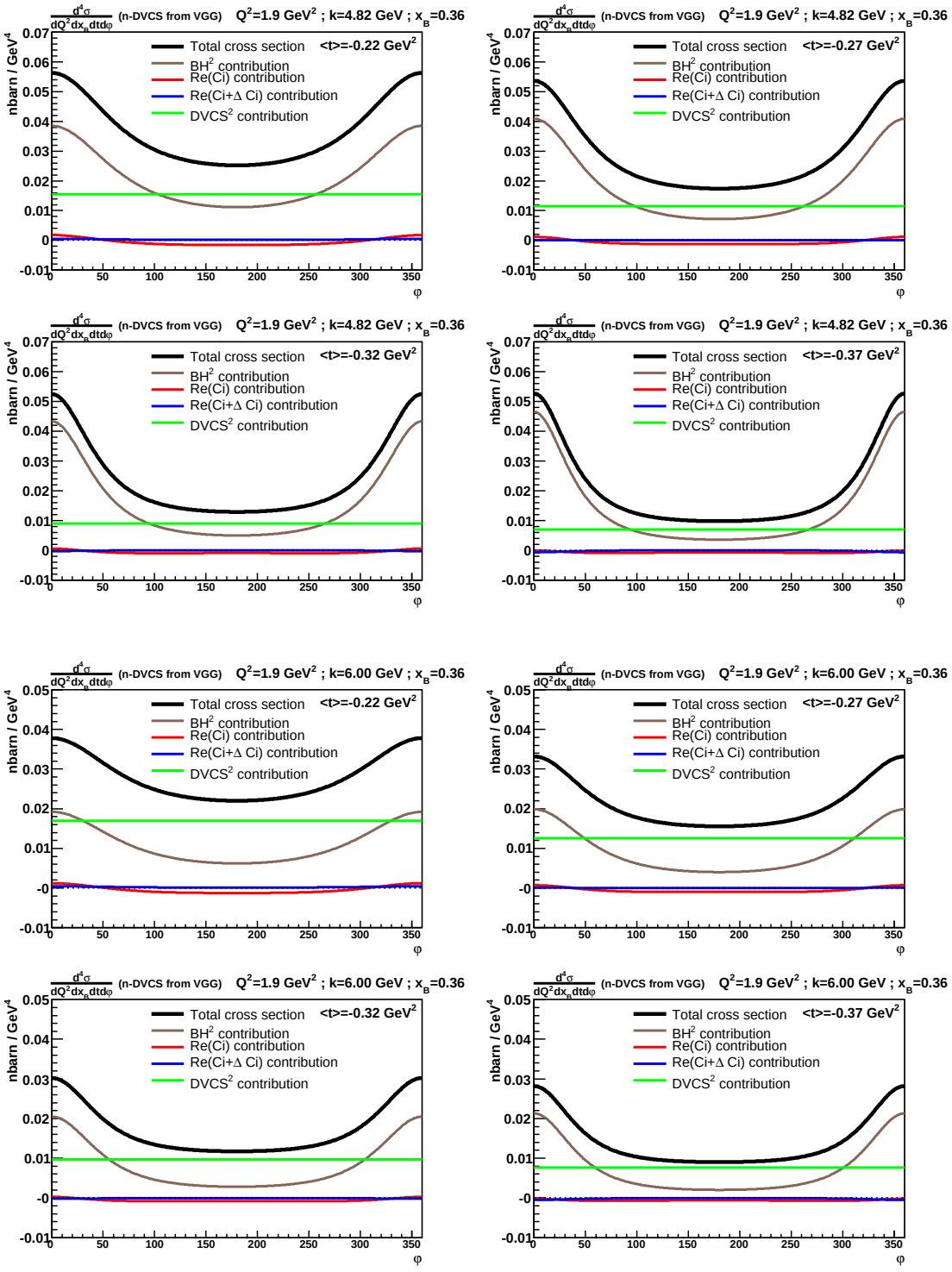

FIG. 6: VGG estimate of the n-DVCS cross sections at 4.82 GeV (top) and 6.0 GeV (bottom) as a function of $\phi_{\gamma\gamma}$ for different t values. The different contributions to the cross sections are shown by the colored curves.

III. DEEP PHOTON ELECTROPRODUCTION ON THE DEUTERON

A. What can be Learned from DVCS on the Deuteron?

The deep photon electroproduction on deuteron in the impulse approximation gives either two nucleons in the final state (that is p-DVCS or n-DVCS) or an intact deuteron. The latter process corresponds to coherent DVCS on the deuteron (d-DVCS) which accesses deuteron GPDs. Since DVCS combines features of both elastic and deep inelastic scattering (DIS), d-DVCS allows for the first time to investigate the partonic structure of deuteron as of a single hadron. From a theoretical point of view, the deuteron is the simplest and best known nuclear system and represents the most appropriate starting point to investigate hard exclusive processes off nuclei. On the other hand, d-DVCS could offer a new source of information about the partonic degrees of freedom in deuteron and access novel nuclear effects not present in DIS on nuclear targets.

The factorization formulas are the same as for nucleon targets [14] and at the leading order in $1/Q^2$, the d-DVCS amplitude is described in terms of nine GPDs : the unpolarized H_i (i=1 to 5) and polarized $\widetilde{H}_i$ (i=1 to 4). At the forward limit, the GPDs $H_{1,5}$ and $\widetilde{H}_1$ are related to deuteron parton distributions, and sum rules analogous to the nucleon ones allow to link the first moment of the GPDs $H_{1,2,3}$ and $\widetilde{H}_{1,2}$ to deuteron form factors [15]. The first moment of the GPDs $H_{4,5}$ and $\widetilde{H}_{3,4}$ are equal to zero which makes it difficult to estimate their t-dependence.

B. Expressions of d-DVCS Polarized Cross Sections

The polarized cross section of d-DVCS have the same harmonic structure as for DVCS on the nucleon, with the same hard scattering kernel but with the appropriate replacement of the hadronic matrix element (deuteron GPDs and FFs instead of nucleon GPDs and FFs). If we assume that the factorization theorem applies for d-DVCS at Q^2=1.9 GeV^2, then the DVCS helicity-independent ($d\sigma$) and helicity-dependent ($d\Sigma$) cross sections read at leading

twist [16]

$$\frac{d^5\sigma}{d^5\Phi} = \frac{d^5\sigma(|BH|^2)}{d^5\Phi} + \Gamma_{DVCS}\,\mathcal{C}_d^{DVCS}(\mathcal{F},\mathcal{F}^*) + \frac{1}{\mathcal{P}_1(\phi_{\gamma\gamma})\mathcal{P}_2(\phi_{\gamma\gamma})}\left(\{\Gamma_0^{\Re} - \cos(\phi_{\gamma\gamma})\Gamma_1^{\Re}\}\Re\mathrm{e}\left[\mathcal{C}_d^I(\mathcal{F})\right] + \Gamma_{0,\Delta}^{\Re}\Re\mathrm{e}\left[\mathcal{C}_d^I + \Delta\mathcal{C}_d^I\right](\mathcal{F})\right) \quad (24)$$

$$\frac{d^5\Sigma}{d^5\Phi} = \frac{1}{\mathcal{P}_1(\phi_{\gamma\gamma})\mathcal{P}_2(\phi_{\gamma\gamma})}\left(\sin(\phi_{\gamma\gamma})\Gamma_1^{\Im}\Im\mathrm{m}\left[\mathcal{C}_d^I(\mathcal{F})\right]\right), \quad (25)$$

where $\Gamma^{\Re,\Im}$ are kinematical factors with no $\phi_{\gamma\gamma}$ dependence [16]. $\Im\mathrm{m}\left[\mathcal{C}_d^I\right]$, $\Re\mathrm{e}\left[\mathcal{C}_d^I\right]$, $\Re\mathrm{e}\left[\mathcal{C}_d^I + \Delta\mathcal{C}_d^I\right]$ and $\mathcal{C}_d^{DVCS}$ represent a combination of deuteron CFFs convoluted with deuteron FFs (except $\mathcal{C}_d^{DVCS}$ which is a bilinear combination of CFFs) and are the coefficients to be extracted from the data. For example, $\mathcal{C}_d^I$ is given by

$$\mathcal{C}_d^I = \left(\mathcal{H}_1 \ldots \mathcal{H}_5\tilde{\mathcal{H}}_1 \ldots \tilde{\mathcal{H}}_4\right)\mathcal{M}\begin{pmatrix} G_1 \\ G_2 \\ G_3 \end{pmatrix} \quad (26)$$

where G_1, G_2 and G_3 are the deuteron elastic FFs and $\mathcal{M}$ is a 9×3 real matrix depending only on ξ and t. $\mathcal{H}_i$ and $\tilde{\mathcal{H}}_i$ are the twist-2 Compton form factors of the deuteron depending on the GPDs H_i and $\widetilde{H}_i$. It should be noticed that the imaginary part of Eq. 26 has been already measured, within the twist-2 approximation, in the previous neutron experiment [18]. The full expressions of the linear combinations of deuteron GPDs $\Delta\mathcal{C}_d^I$ and the bilinear combination $\mathcal{C}_d^{DVCS}$ are given in reference [16].

C. Separation of the Interference and the DVCS^2 Terms

As in the neutron case, the separation of the interference and the DVCS^2 terms is impossible with a single beam energy. The Γ factors in Eq. 24 have the same beam energy dependence as those in Eq. 17 since they differ only by the target mass. Therefore, running at the two proposed beam energies will allow to perform a clean separation of the interference and the DVCS^2 terms, within the twist-2 approximation. $\mathcal{C}_d^{DVCS}$ is kinematically suppressed by at least a factor 50 in our kinematics relatively to the interference terms $\Re\mathrm{e}\left[\mathcal{C}_d^I\right]$ and $\Re\mathrm{e}\left[\mathcal{C}_d^I + \Delta\mathcal{C}_d^I\right]$. However, its contribution to the cross section might be important due to a large value of this term according to a model estimate of deuteron GPD [15, 17] (see next section).

D. Deuteron GPD Model Estimates

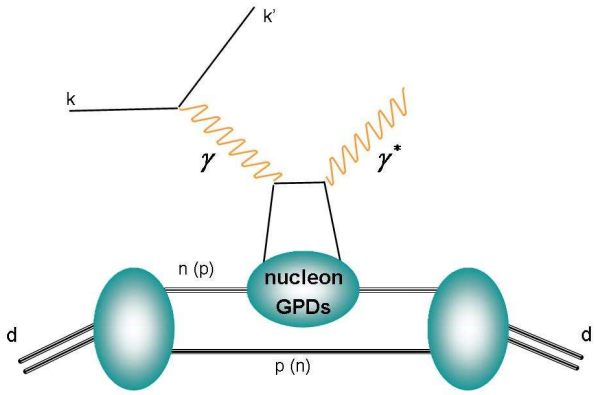

FIG. 7: Coherent DVCS on the deuteron in the impulse approximation. The virtual photon interacts with a parton inside the nucleon, the other nucleon being spectator. Both nucleons recombine to re-form the deuteron in the final state.

Most of the models for the nucleon GPDs exploit the GPD relationship with form factors and parton distributions, supplemented with some assumptions about the ξ dependence. In the deuteron case, little is known experimentally about axial form factors or one of the parton distributions (b_1) which makes their parametrization difficult. In addition, four GPDs have vanishing first moments and then no information can be inferred about their t-dependence. To ride out these difficulties, the easiest way consists to use an impulse approximation where only one nucleon is active and participates in the absorption and emission of the photon (see Fig. 7). The deuteron GPDs are then a convolution of the nucleon GPDs with the two-nucleon light-cone wave function of the deuteron [15, 17]. In the model by F. Cano and B. Pire, only the nucleon GPDs H and $\widetilde{H}$ are considered since E and $\widetilde{E}$ go with suppressing kinematical prefactors [17]. Figure 8 shows an estimate of the deuteron GPD combinations at our kinematics. According to this model, the $\mathcal{C}^{DVCS}$ term is, here also, at least 100 times bigger than the interference terms $\Re\mathrm{e}\left[\mathcal{C}^I\right]$ and $\Re\mathrm{e}\left[\mathcal{C}^I + \Delta\mathcal{C}^I\right]$. The rapid decrease as a function of $|t|$ is expected from the behavior of the deuteron form factors.

Figure 9 shows the expected coherent DVCS cross sections off the deuteron for the two requested beam energies, as well as the different contributions to the cross section. As expected from Fig. 8, the DVCS^2 has a significant contribution to the cross section. Notice that at $\phi_{\gamma\gamma}$=180°, even the BH contribution becomes negligible and we measure mainly the

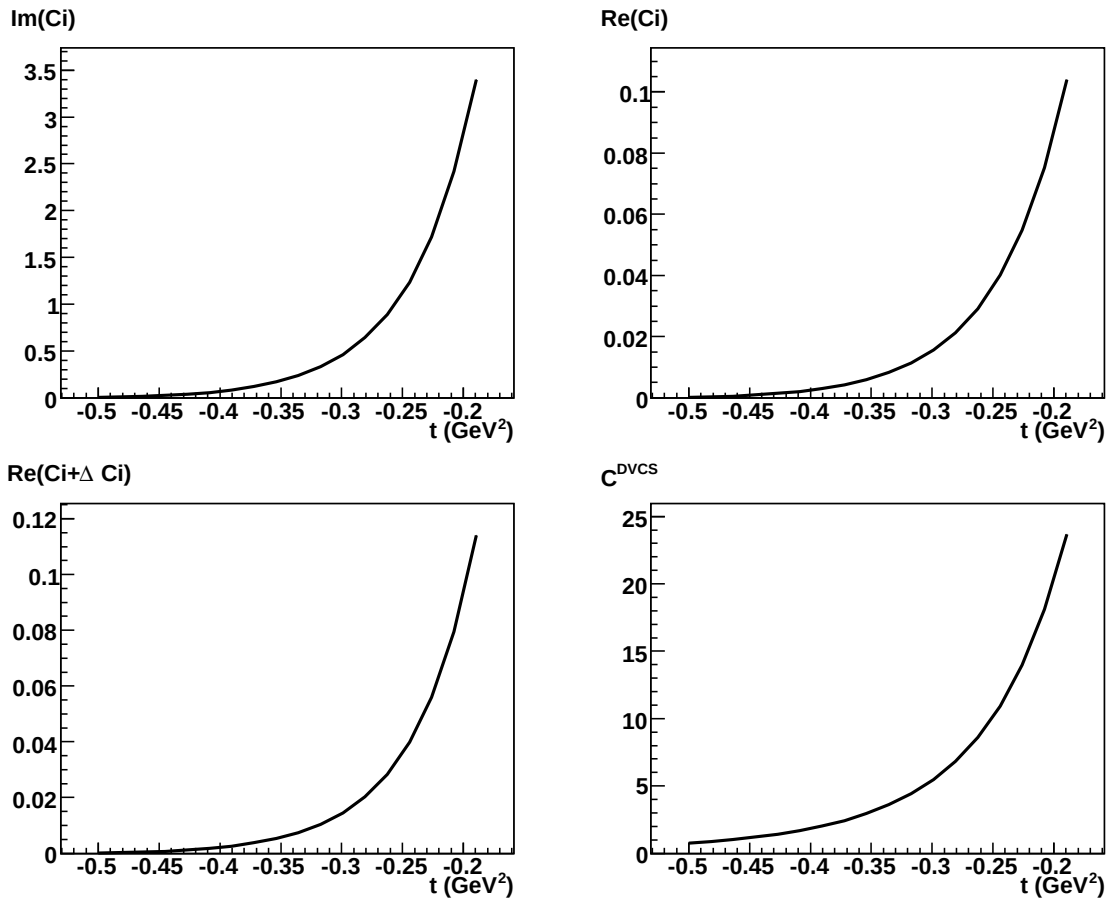

FIG. 8: Calculation of the deuteron observables to be extracted from the data at our kinematics [17].

DVCS^2 contribution.

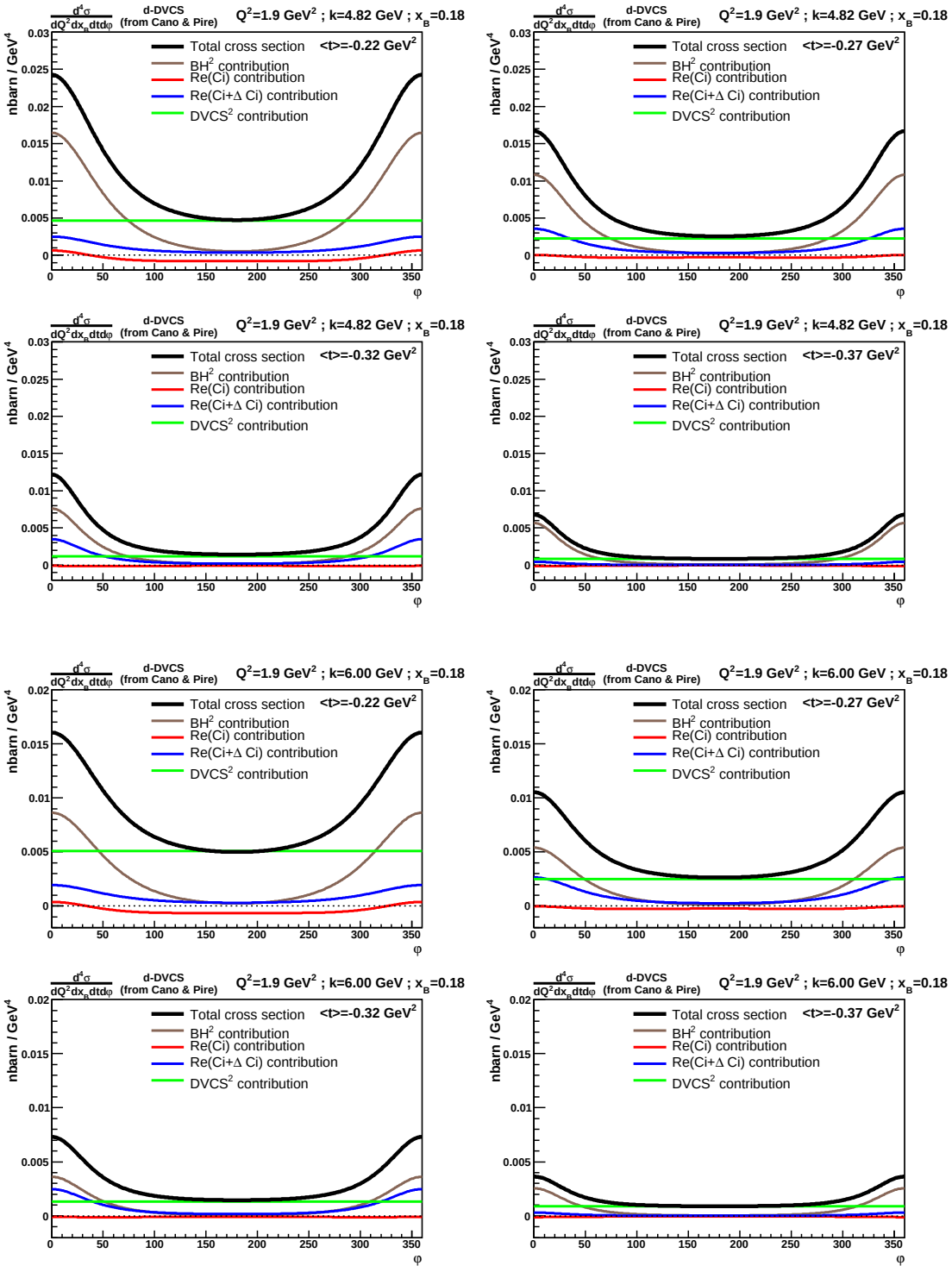

FIG. 9: Cano and Pire model [17] estimates of the d-DVCS cross sections at 4.82 GeV (top) and 6.0 GeV (bottom) as functions of $\phi_{\gamma\gamma}$ for four t values. The different contributions to the cross sections are shown by the colored curves.

IV. DEEP π^0 ELECTROPRODUCTION OFF THE NEUTRON

The π^0 electroproduction longitudinal cross section provides an extremely interesting access to GPDs. Indeed, if the twist-2 contribution dominates the cross section, it provides a promising way to perform a flavor separation of GPDs. Moreover, π^0 production probes only the "polarized" GPDs of the nucleon ($\tilde{H}$ and $\tilde{E}$), which contain information about the spatial distribution of the quark spin. This complements DVCS measurements, where all GPDs participate.

At leading twist

$$\frac{d\sigma_L}{dt} = \frac{1}{2}\Gamma \sum_{h_N, h_{N'}} |\mathcal{M}^L(\lambda_M = 0, h'_N, h_N)|^2 \propto \frac{1}{Q^6} \qquad \frac{d\sigma_T}{dt} \propto \frac{1}{Q^8} \tag{27}$$

with

$$\mathcal{M}^L \propto \left[\int_0^1 dz \frac{\phi_\pi(z)}{z}\right] \int_{-1}^1 dx \left[\frac{1}{x-\xi} + \frac{1}{x+\xi}\right] \left\{\Gamma_1 \widetilde{H}_{\pi^0} + \Gamma_2 \widetilde{E}_{\pi^0}\right\}(x, \xi, t) \tag{28}$$

The Γ factors in Eq. (27) and Eq. (28) are kinematics factors and ϕ_π is the pion distribution amplitude. The flavor combination of GPDs entering in Eq. (28) is different from that in DVCS on the nucleon. Indeed,

$$|\pi^0\rangle = \frac{1}{\sqrt{2}}\{|u\bar{u}\rangle - |d\bar{d}\rangle\} \qquad \widetilde{H}_{\pi^0} = \frac{1}{\sqrt{2}}\left\{\frac{2}{3}\widetilde{H}^u + \frac{1}{3}\widetilde{H}^d\right\}, \tag{29}$$

whereas in DVCS on the proton and neutron:

$$\begin{aligned} |p\rangle &= |uud\rangle, \qquad H^{(p)}_{DVCS} = \frac{4}{9}H^u + \frac{1}{9}H^d\,, \\ |n\rangle &= |udd\rangle, \qquad H^{(n)}_{DVCS} = \frac{1}{9}H^u + \frac{4}{9}H^d\,. \end{aligned} \tag{30}$$

In the neutron case, we have applied isospin symmetry, and defined the flavor GPDs $H^{u,d}$ in terms of the proton flavor contributions.

As in the case of the DVCS unpolarized cross section, with these measurements we access a GPD integral over x. Note that at twist-2 level, the pion distribution amplitude $\phi_\pi(z)$ enters only as a normalization integral. Note also that the amplitude of Eq. (28) enters squared in the cross section. Therefore, a bilinear combination of these GPD integrals are measured.

The differential π^0 electroproduction cross section reads:

$$\frac{d\sigma}{dt} = \frac{d\sigma_T}{dt} + \epsilon\frac{d\sigma_L}{dt} + \sqrt{2\epsilon(1+\epsilon)}\frac{d\sigma_{LT}}{dt}\cos\phi + \epsilon\frac{d\sigma_{TT}}{dt}\cos 2\phi + \lambda\sqrt{2\epsilon(1-\epsilon)}\frac{d\sigma_{LT'}}{dt}\sin\phi \tag{31}$$

where λ is the electron helicity and where the virtual photon polarization is given by:

$$\epsilon = \left(1 + 2\frac{|\mathbf{q}|^2}{Q^2}\tan^2\frac{\theta}{2}\right)^{-1}. \tag{32}$$

Along with DVCS cross sections, E00-110 also measured the exclusive π^0 electroproduction cross section off the proton in the deep inelastic regime. Figure 10 shows preliminary results. Similar results on the neutron could not be extracted from E03-106 due to a high photon threshold caused by radiation damage of the calorimeter. Only an upper limit of $\sigma(n)/\sigma(p) < 0.5$ for exclusive π^0 electroproduction could be set in E03-106 [18]. Also, since only one beam energy was used, we could not perform a Rosenbluth separation to extract the longitudinal cross section that is related to GPDs in leading twist.

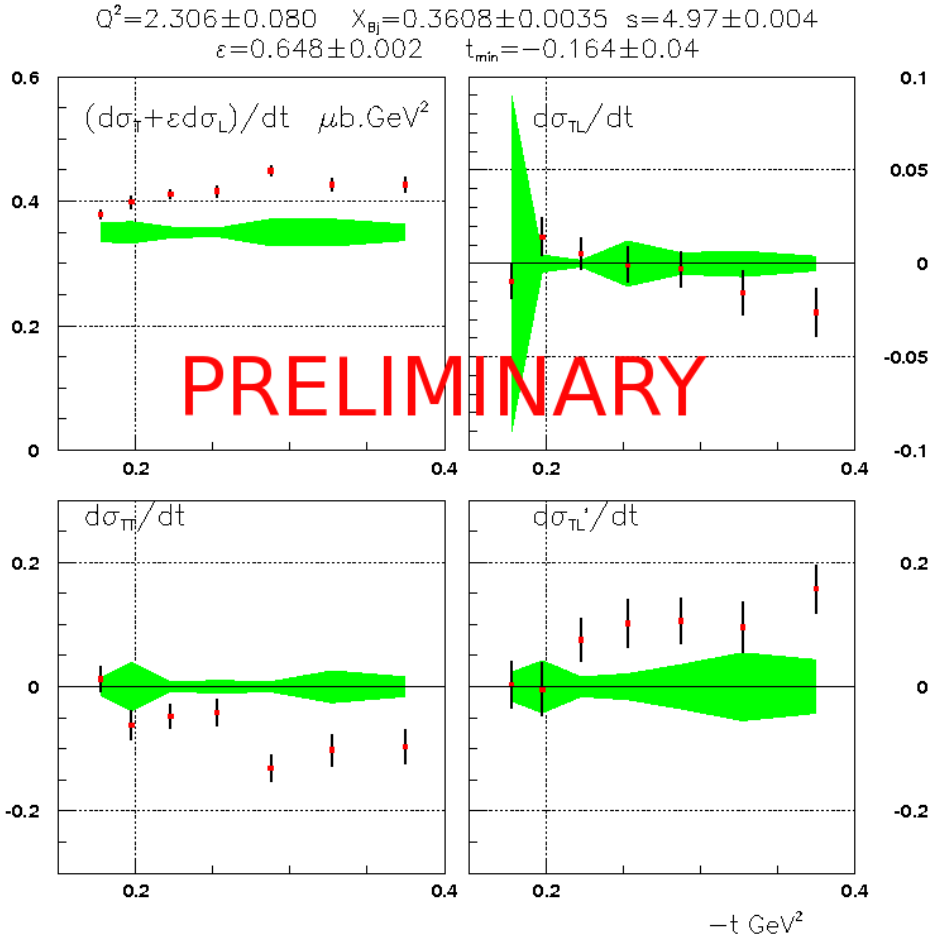

FIG. 10: Cross sections of π^0 electroproduction off the proton at Q^2=2.3 GeV^2: preliminary results from E00-110. Green bands represent systematic errors.

This new experiment not only will provide a measurement of the π^0 cross section off the neutron, but also will separate the longitudinal and transverse cross sections using the Rosenbluth technique and two different beam energies. A scaling test of the longitudinal component on the proton will be performed during E07-007. The cross section on the neutron is expected small. Figure 11 shows an estimate by Eides, Frankfurt and Strikman [23] of the ratio of longitudinal cross sections off the proton and off the neutron in the deep virtual limit.

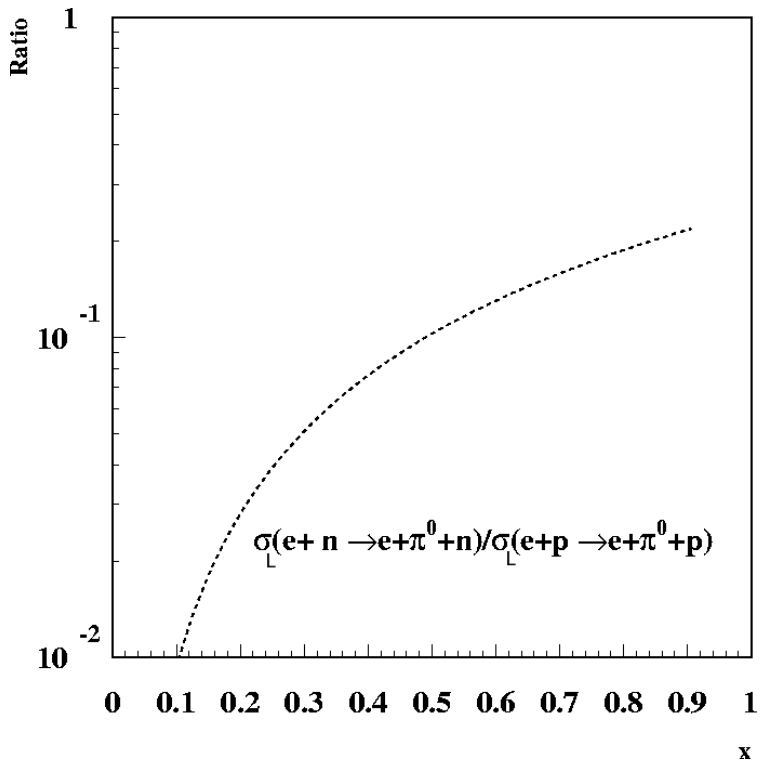

FIG. 11: The x dependence of the ratio $\sigma_L(\gamma_L + n \to \pi^0 + n)/\sigma_L(\gamma_L + p \to \pi^0 + p)$ from [23] for the proton and neutron targets. At $x_B = 0.36$ the cross section off the neutron is predicted ≈ 13 times smaller than off the proton.

V. EXPERIMENTAL SETUP

The experimental apparatus is mainly the same as in the previous DVCS experiments in Hall A. However, a few experimental upgrades are necessary to reduce the large systematic errors of E03-106. **These modifications are common to both the future proton experiment (E07-007) and the proposed one, and are already planned for the former. Therefore, the proposed experiment, planned to run simultaneously with the proton experiment, does not require any additional apparatus.** This section briefly summarizes the experimental setup and mainly concentrates on the upgrades. Further details can be found in reference [19].

A. Targets

We will use the standard 15 cm liquid deuterium target (LD2). During the data taking of E07-007 at the proposed kinematics, we will perform frequent swaps between LD2 and LH2, approximately a swap every 4 hours. In E03-106, almost one month separated the LD2 and LH2 data taking and the calorimeter calibration had changed during that period because of the radiation damage of the calorimeter blocks. In spite of the offline (re)calibration of data with two independent methods (cf. section VI A), we noticed a 1% systematic uncertainty on the calibration between H_2 and D_2 data. This 1% uncertainty led to a very large systematic error on the neutron results because our analysis method is based on an accurate subtraction of H_2 data from D_2 data. This systematic affected significantly our previous measurement of the unpolarized cross sections. However, the measured helicity dependent cross sections were compatible with zero, so even with a large relative systematic, the results were still relevant and accurate enough to constrain GPD models. In the proposed experiment, the frequent swap between LH2 and LD2 will reduce by a factor 25 the systematic error due to the relative calibration between H_2 and D_2 data. Indeed, we have learned from E03-106 and E00-110 that the calibration of the most radiation-exposed calorimeter blocks will not vary by more of 0.04% in 4 hours.

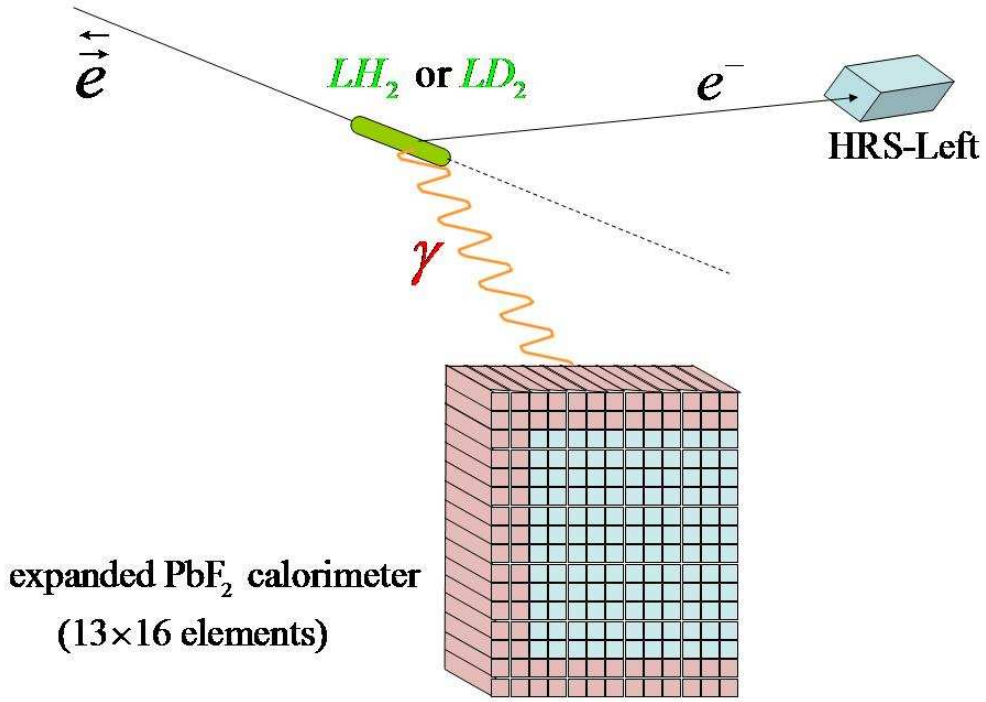

FIG. 12: Schematic of the DVCS setup for the proposed experiment. The scattered electron is detected in the HRS and the photon is detected in the expanded calorimeter.

B. DVCS Detectors

We will detect the scattered electrons at θ_e=18.13° in the left HRS. The DVCS photons will be detected in an electromagnetic calorimeter, placed at 1.10 m from the target, centered around the direction of the virtual photon at θ_{γ^*}=−18.45°, and covering the t acceptance -0.5 GeV$^2 < t$.

We will use the calorimeter of the previous DVCS experiments with a 50% expansion : 76 PbF_2 blocks (3×3 cm^2×20X$_0$) will be added to reach a structure of 13×16 elements instead of the 11×12 elements previously (see Fig. 12). The main goal of this expansion is to detect enough photons from π^0 symmetric decays at high $-t$ in order to match the DVCS acceptance and subtract properly the π^0 contamination.

In E03-106, we used two recoil detectors in order to detect and tag the recoil nucleon charge. However, we found that a double coincidence analysis (calorimeter + HRS) can successfully identify the DVCS events with the missing mass technique [13]. In addition, the recoil detector limited the experimental acceptance. We will therefore not use a recoil

detector in this new experiment, as it will also be the case in E07-007. The coherent deuterium and quasi free nucleon events overlap kinematically, but are separated on average by a missing mass offset of $t/2$.

C. Neutral Pion Detection and Background Subtraction

Neutral pion $eD \rightarrow e'\pi^0 X$ events will generate both double $\mathrm{D}(e,e'\gamma)\gamma X$ and triple $\mathrm{D}(e,e'\gamma\gamma)X$ events. The latter events will be used to determine the π^0 electroproduction cross sections. The former are an irreducible background to DVCS, and must be estimated from the latter. The $\pi^0 \rightarrow \gamma\gamma$ decay is isotropic in the pion rest frame. Therefore, with a high statistics sample of $\mathrm{D}(e,e'\gamma\gamma)X$ events, it is possible, within a Monte Carlo simulation, to compute an accurate estimate of the background $\mathrm{D}(e,e'\gamma)\gamma X$ events. For exclusive π^0 production, there is a strong forward boost of the decay toward the calorimeter. For 50% of all π^0 decays, the two photons both have lab energy greater than $E_\pi/4$ and lie within a cone of half-angle $\sqrt{3}m_\pi/E_\pi$. The calorimeter expansion and the modification to the trigger ensure a large double-photon acceptance for all exclusive or near exclusive π^0 events (typically $> 50\%$) within the projected t-range.

D. Trigger and Electronics

The acquisition system is roughly the same as in the previous DVCS experiments. It is based on the 1 GHz Analog Ring Sampler (ARS) which digitizes the PMT signals with an analog memory chip in 128 samples (one sample per nanosecond). Figure 13 shows an example of ARS output representing two different pulses which can be separated offline with a wave form analysis. The pile-up rate in the ARS affects directly the calorimeter resolution and represents the limiting factor for the beam current. In the proposed experiment we will run at the maximal beam current of E03-106: 4 μA, leading to a luminosity of $4{\cdot}10^{37}$ cm^{-2}s^{-1}.

In E00-110 and E03-106, a specific trigger was used to minimize the number of ARS channels for readout at each event, and hence the acquisition deadtime. It starts by computing all overlapping ADC sums of 4 adjacent blocks in the calorimeter, then looks for at least one sum over a programmable threshold set to 1.2 GeV equivalent in E03-106. In our kinematics, the energy of a DVCS photon or an exclusive π^0 (from $\mathrm{N}(e,e'\pi^0)\mathrm{N}$) is around 2.7 GeV. As

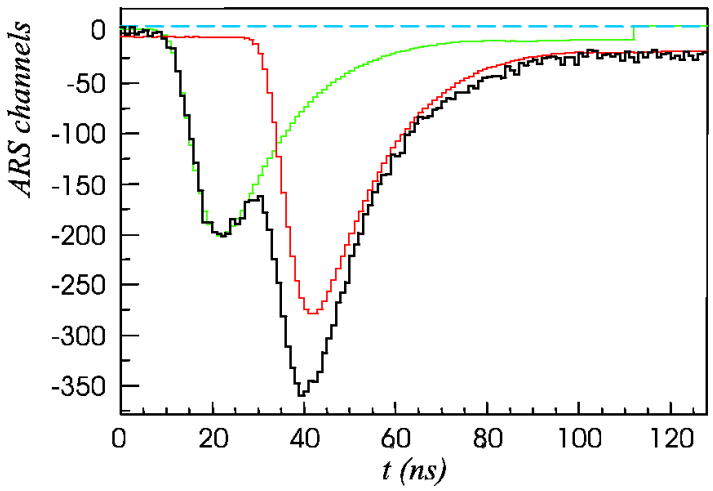

FIG. 13: ARS output signal showing a two-pulse pile-up event.

mentioned before, one needs to detect photons coming from symmetric π^0 decays in order to remove the π^0 contamination. These photons have roughly half of the π^0 energy (1.35 GeV) and could be recorded, in principle, with the 1.2 GeV trigger threshold. Unfortunately, the radiation damage of some calorimeter blocks led to a higher effective trigger threshold that prevented the recording of enough π^0 events. The π^0 contamination in E03-106 was treated consequently as a systematic error.

In the proposed experiment (and E07-007) we are planning to modify the trigger logic in order to properly record π^0 events. The new trigger will compute the ADC sum of all the calorimeter blocks then record all the ARS channels if the sum is higher than a programmable threshold, typically 2 GeV threshold. This new method has the advantage to record all the calorimeter blocks regardless of the number of clusters (DVCS or π^0 photons) and their corresponding energies. Note that a 2 GeV threshold will decrease the data record rate and thus will not increase the experimental deadtime in spite of the large number of readout channels. In addition, faster electronics will be used to improve the data record and transfer. However, one must pay attention to the radiation damage in order to avoid the E03-106 scenario. In fact, we are planning to cure the calorimeter periodically with blue light in order to keep a good optical transmission in all blocks and hence a stable gain [19]. We expect with these modifications less than 2% accuracy on the determination of π^0 contamination.

VI. ANALYSIS TECHNIQUE

The data analysis will be similar to the one performed in E03-106 [18]. However, the method for extracting the DVCS observables will be slightly modified to take into account the two beam energies. Let us describe briefly the main features of this analysis.

A. Calorimeter Calibration

We will calibrate the electromagnetic calorimeter via the elastic H$(e, e'p)$ reaction where the proton is detected in the HRS and the scattered electron in the calorimeter. This calibration serves also to check the geometrical surveys of the calorimeter and the spectrometer and will be performed periodically during the experiment. Two calibration methods based on two independent reactions, recorded simultaneously with the DVCS data, will then be used to continuously monitor the elastic calibration :

- The first method is based on the reconstructed π^0 mass with two detected photons in the calorimeter. The comparison between the pion mass and the position of the invariant mass peak (Fig. 14 left) for different regions in the calorimeter allows us to identify mis-calibrated blocks.

- The second method is based on the identification of n$(e, e'\pi^-)$p events through the missing mass of D$(e, e'\pi^-)$X where the π^- is detected in the HRS and the scattered electron in the calorimeter (Fig. 14 right). Here again, the position of the peak corresponding to n$(e, e'\pi^-)$p events allows us to monitor and correct the calibration of the calorimeter blocks. Note that this calibration method can only be applied to D_2 data.

We expect 1%, or less, uncertainty on the calorimeter (absolute) calibration. However, the difference between the calibration of H_2 and D_2 data is expected to be less than 0.04% as mentioned in section V A. This quantity is more relevant than the absolute calibration since it affects strongly the systematic errors of the results.

B. The Impulse Approximation

Since the momentum transfer to the recoil DVCS nucleon is large compared the momentum distribution of the nucleons inside the deuteron, we expect the DVCS reaction to be

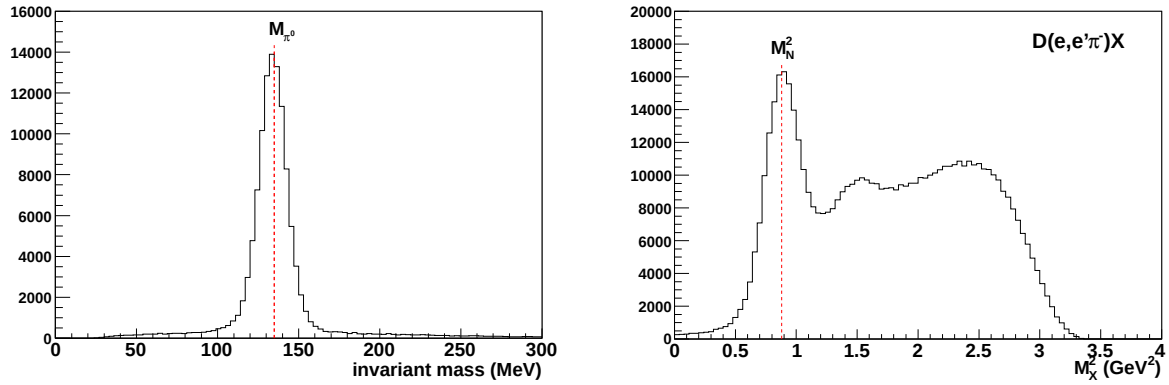

FIG. 14: Left : invariant mass of two detected photons in the calorimeter; the peak corresponds to photons coming from symmetric π^0 decays in the lab frame. Right : the missing mass squared of D$(e, e'\pi^-)$X events; the peak corresponds to n$(e, e'\pi^-)$p events. The two spectra are obtained from E03-106 data.

well described by the impulse approximation (IA), where the virtual photon scatters on a quasi-free nucleon, the other one acting as a spectator. Figure 15 shows the Fermi momentum distribution together with the momentum distribution of the DVCS recoil particle in the proposed kinematics. The overlap between these distributions is less than 3%. This means the plane wave description of the final state is orthogonal to the bound deuteron, making final state interaction effects between a pn pair small. Thus, the inclusive yield on a deuterium target can be expressed as:

$$\begin{aligned} \mathrm{D}(\vec{e}, e'\gamma)X &= d(\vec{e}, e'\gamma)d + n(\vec{e}, e'\gamma)n + p(\vec{e}, e'\gamma)p + \ldots \\ &= \text{d-DVCS} + \text{n-DVCS} + \text{p-DVCS} + \ldots \end{aligned} \tag{33}$$

where the "..." denotes meson production channels.

C. Selection of DVCS Events

The selection of DVCS events will be performed with the missing mass of D,H$(e, e'\gamma)$X events with coincident electron-photon detection. Figure 16 shows the missing mass squared M_X^2 of D$(e, e'\gamma)$X events, from E03-106 data, after subtraction of an accidental coincidence sample. Since the missing mass is calculated with a target mass equal to the nucleon mass (M_N), n-DVCS and p-DVCS events are around M_N^2 in Fig. 16 while d-DVCS events are

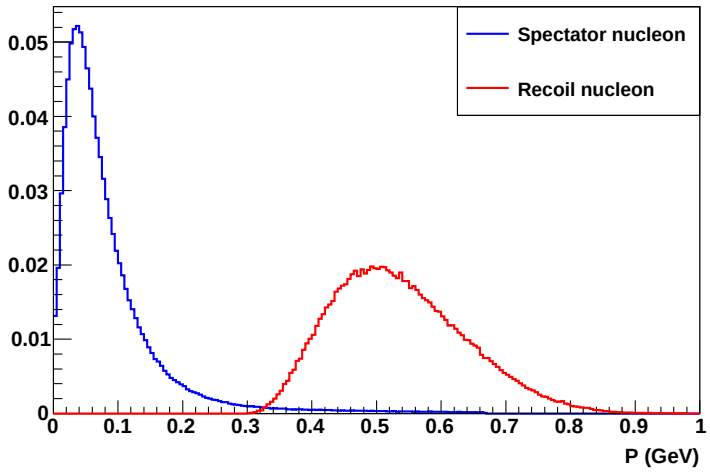

FIG. 15: Normalized momentum distributions of the spectator proton (blue) in the deuteron (Fermi momentum distribution) and the n-DVCS recoil neutron (red) in the proposed kinematics. The overlap between these distributions is less than 3%.

around $M_N^2 + t/2$. Indeed,

$$\begin{aligned} M_X^2 &= (p + q - q')^2 \\ &= M_N^2 + t + 2p\,(q - q') \\ &= M_N^2 + t + 2M_N\,(q_0 - q'_0) \end{aligned} \tag{34}$$

where q_0 (q'_0) is the real (virtual) photon energy. On the other hand, the momentum transfer t for a d-DVCS reaction is given as a function of the deuteron mass M_d by :

$$t = (p - p')^2 = -2M_d\,(q_0 - q'_0) \qquad \text{since} \quad p'_0 = M_d + q_0 - q'_0\,. \tag{35}$$

Using Eq. 34 and Eq. 35, we find :

$$M_X^2 = M_N^2 + t - \frac{M_N}{M_d} t \approx M_N^2 + t/2\,. \tag{36}$$

We find also in the missing mass spectrum of D$(e, e'\gamma)\gamma$ X events, coming from π^0 decays, starting at M_N^2 and which was not subtracted in the spectrum of Fig. 16. Finally, the meson production channels starts at the pion production threshold $(M_N + M_{\pi^0})^2$ and will be strongly suppressed by the cut $M_X^2 < (M_N + M_{\pi^0})^2$. Therefore, under the missing mass cut and after the subtraction of π^0 contamination as proposed in this experiment, we will find only the p-DVCS, n-DVCS and d-DVCS events. A similar analysis with H$(e, e'\gamma)$X events from Fermi-broadened H_2 data allows to subtract the p-DVCS contribution to have finally only n-DVCS and d-DVCS events under the missing mass cut.

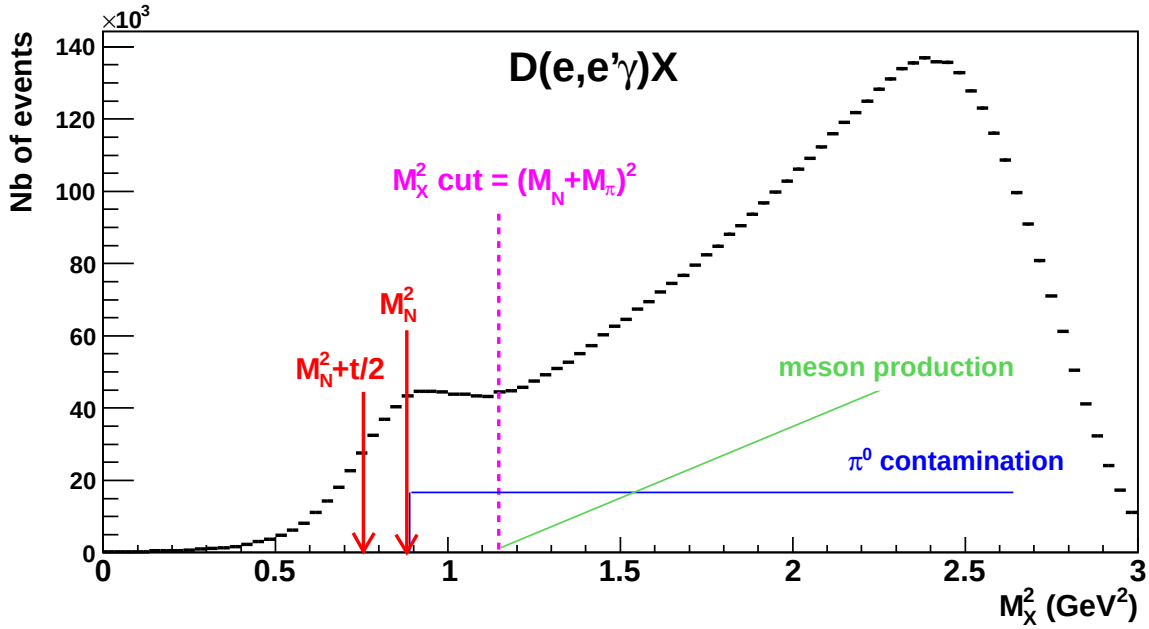

FIG. 16: The missing mass squared of D$(e,e'\gamma)$X events after accidentals subtraction. The red arrows show the average position of n-DVCS, p-DVCS and d-DVCS events : N-DVCS events are around M_N^2 while d-DVCS events are around $M_N^2 + t/2$. The colored lines show the "range" of meson production and π^0 contamination events. The dashed line shows the missing mass cut.

D. Extraction of DVCS Observables

The extraction of the DVCS observables is based on the Belitsky-Kirchner-Mueller formalism of the cross sections [16, 20]. After the selection of $n + d$-DVCS events for the two data sets (4.82 GeV and 6.0 GeV) as described above, we write the experimental cross section as the sum of Eq. 17 and Eq. 24:

$$\frac{d^6\sigma^{exp}}{d^5\Phi dM_X^2} = \frac{d^5\sigma_d}{d^5\Phi}\cdot\frac{df_d}{dM_X^2} + \frac{d^5\sigma_n}{d^5\Phi}\cdot\frac{df_n}{dM_X^2}, \tag{37}$$

where the factors $df_{d,n}$ are the resolution, radiative, and kinematic smeared missing mass distributions for coherent deuterium and quasi-free neutron DVCS events, respectively. Keeping only twist-2 terms, the neutron and deuteron cross sections are

$$\begin{aligned}
\frac{d^5\sigma_n}{d^5\Phi} &= \frac{d^5\sigma(|BH|_n^2)}{d^5\Phi} \\
&+ \Gamma_n^{DVCS}\,\mathcal{C}_n^{DVCS} + \frac{1}{\mathcal{P}_1\mathcal{P}_2}\left(\{\Gamma_{0,n}^{\Re} - \cos(\phi_{\gamma\gamma})\Gamma_{1,n}^{\Re}\}\Re\mathrm{e}\left[\mathcal{C}_n^I\right] + \Gamma_{0,\Delta,n}^{\Re}\Re\mathrm{e}\left[\mathcal{C}_n^I + \Delta\mathcal{C}_n^I\right]\right) \\
\frac{d^5\sigma_d}{d^5\Phi} &= \frac{d^5\sigma(|BH|_d^2)}{d^5\Phi} \\
&+ \Gamma_d^{DVCS}\,\mathcal{C}_d^{DVCS} + \frac{1}{\mathcal{P}_1\mathcal{P}_2}\left(\{\Gamma_{0,d}^{\Re} - \cos(\phi_{\gamma\gamma})\Gamma_{1,d}^{\Re}\}\Re\mathrm{e}\left[\mathcal{C}_d^I\right] + \Gamma_{0,\Delta,d}^{\Re}\Re\mathrm{e}\left[\mathcal{C}_d^I + \Delta\mathcal{C}_d^I\right]\right).
\end{aligned} \tag{38}$$

Six observables will be fit for each t bin (highlighted in red in Eq. 38). We minimize:

$$\chi^2 \;=\; \sum_i \left[\left(Y_i^{\rm Exp} - Y_i^{\rm Fit} \right)^2 / \sigma_i^2 \right]. \tag{39}$$

The $Y_i^{\rm Exp}$ are the experimental yields, after accidental and π^0 subtractions, in bin i, with statistical errors σ_i. The fit yields, $Y_i^{\rm Fit} = \sum_\Gamma \mathcal{C}_\Gamma K_\Gamma(i)$, depend linearly on the fitting harmonics $\mathcal{C}_\Gamma$ and the Monte-Carlo integrated kinematic weights:

$$K_\Gamma(i) \;=\; \mathcal{L} \sum_{j=1}^{N^{\rm sim}} \frac{\Delta^3\Phi_e \Delta^2\Phi_\gamma(j)}{N^{\rm sim}} \Gamma_\Gamma(j) \eta(i,j). \tag{40}$$

$\mathcal{L}$ is the integrated experimental luminosity and $N^{\rm sim}$ is the total number of events in the simulation. The phase-space factors are $\Delta^3\Phi_e = \Delta Q^2 \Delta x_{\rm Bj} \Delta\phi_e$ and $\Delta^2\Phi_\gamma = 2\pi[t_{\rm min}(Q^2, x_{\rm Bj}) - t_{\rm max}]$. The indicator function $\eta(i,j) = 1$ if simulation event j lands in experimental bin i, otherwise, $\eta(i,j) = 0$.

The simulation takes into account the detectors acceptance and resolution and it includes both external and real internal radiative effects. Virtual radiative corrections will be applied as a correction factor to each experimental bin (depending on $\phi_{\gamma\gamma}$ and t), following recent work by Guichon, based on [24] using a GPD model [21] for the VCS amplitude. These corrections differ at most 2% bin-to-bin relative to the global radiative corrections previously applied.

The binning is performed on 4 experimental variables :

- The $\phi_{\gamma\gamma}$ angle, in order to separate the $\cos(\phi_{\gamma\gamma})$ contributions in Eq. 38.
- The M_X^2 variable, in order to separate the neutron (2^{nd} line of Eq. 38) from the deuteron contribution (4^{th} line of Eq. 38).
- The transfer t, in order to study the t-dependence of the extracted coefficients.
- The beam energy, in order to separate the BH-DVCS interference term from the pure DVCS^2 contribution

VII. PROPOSED KINEMATICS AND BEAM TIME REQUEST

Table I summarizes our proposed kinematics and beam time request. Among the three kinematics of E07-007, we propose the one at Q^2=1.9 GeV^2 (2^{nd} kinematics of E07-007) which is also the same kinematics of the previous neutron experiment.

We request approximately three times more integrated luminosity for LD2 target than LH2 target because the n-DVCS cross section is expected to be, at least from the BH behavior, three times smaller than the p-DVCS cross section. We have learnt from E03-106 that the beam current affects strongly the experimental resolution. Consequently, the proposed beam current will be 4μA, the maximal value in E03-106 and E07-007, leading to 400 hours of requested beam time (200 hours for each beam energy). 144 hours for the experimental calibration (72 hours) and the calorimeter curing (72 hours) are already planned for E07-007.

	LH_2 target **E07-007**		LD_2 target	
Q^2 (GeV^2)	1.9		1.9	
x_B	0.36		0.36	
W^2 (GeV^2)	4.26		4.26	
q' (GeV)	2.73		2.73	
k (GeV)	6.00	4.82	6.00	4.82
k' (GeV)	3.19	2.01	3.19	2.01
θ_e (deg)	18.13	25.60	18.13	25.60
θ_q (deg)	-18.45	-16.07	-18.45	-16.07
θ_{Calo} (deg)	-18.45	-16.23	-18.45	-16.23
Beam time (h)	30	90	**200**	**200**
Total beam time requested : 200 h + 200 h = **400 h**				

TABLE I: Proposed kinematics and beam time request. k (k') is the incident (scattered) electron energy; q' is the virtual photon energy; θ_e (θ_q) is the scattered electron (photon) angle respectively to the beam.

VIII. PROJECTED RESULTS

In order to compute the projected results of n-DVCS and d-DVCS, we used the model estimates described in sections III D and II D and the requested luminosity of Tab I. Figure 17 shows the expected sum of n-DVCS and d-DVCS cross sections as a function of $\phi_{\gamma\gamma}$ and for different values of the transfer t. According to models, the difference between the expected cross sections and the known BH contribution of the neutron and the deuteron (also shown in Fig. 17) is mainly due to the DVCS^2 contribution. We expect a 5% relative systematic error on the results which is at least a factor 2 smaller than the statistical error bars (see Fig. 17). The different contributions of systematic uncertainties are summarized in Tab. II.

Type		Relative errors (%)	
		E03-106	proposed
Luminosity	target length and beam charge	1	1
HRS-Calorimeter	Drift chamber multi-tracks	1.5	1.5
	Acceptance	2	2
	Trigger dead-time	0.1	0.1
	H_2 and D_2 relative calibration	~ 40	2
DVCS selection	π^0 subtraction	~ 30	2
	e(p,e'γ)πN contamination	2	2
	radiative corrections	2	2
Total cross section sum		~ 50	5

TABLE II: Relative systematic error budget for E03-106 and for the proposed experiment.

Using the procedure described in section VI D, one can extract from the unpolarized cross sections the six n-DVCS and d-DVCS observables : $\Re\mathrm{e}\left[\mathcal{C}^I_{n,d}\right]$, $\Re\mathrm{e}\left[\mathcal{C}^I_{n,d}+\Delta\mathcal{C}^I_{n,d}\right]$ and $\mathcal{C}^{DVCS}_{n,d}$. The expected results for these coefficients and the expected improvement of the corresponding systematic errors are shown in Fig. 18. Error bars of Fig. 18 are not purely statistics (i.e depending on the total number of counts) but depend strongly on the correlation between the n-DVCS and d-DVCS contributions. At small $|t|$ for example, the kinematical separation of $t/2$ on the missing mass variable between n-DVCS and d-DVCS leads to a larger

error bar in spite of a higher absolute statistics. This correlation, and hence error bars, depends on the experimental resolution. The results of Fig. 18 are obtained assuming the same experimental resolution of E03-106. The following precautions will be taken in order to keep (and probably improve) this resolution level :

- The beam current will never exceed $4\mu A$: the maximal beam current of E03-106.
- The calorimeter blocks will be periodically cured from radiation damage which was not done in E03-106. That will keep a good light transmission in the blocks and therefore a large number of collected photo-electrons in PMTs.
- The calorimeter calibration will be performed by elastic H$(e, e'p)$ data taken several times during the experiment. This calibration will be continuously monitored with H,D$(e, e'\pi^0)$ and D$(e, e'\pi^-)p$ reactions.

A measurement of the helicity-dependent cross section will also be done in the proposed experiment. The expected statistics will approximately be the same as in E03-106 but the systematics will be reduced by at least a factor 10. That will lead to a factor 2 improvement of this measurement with respect to E03-106.

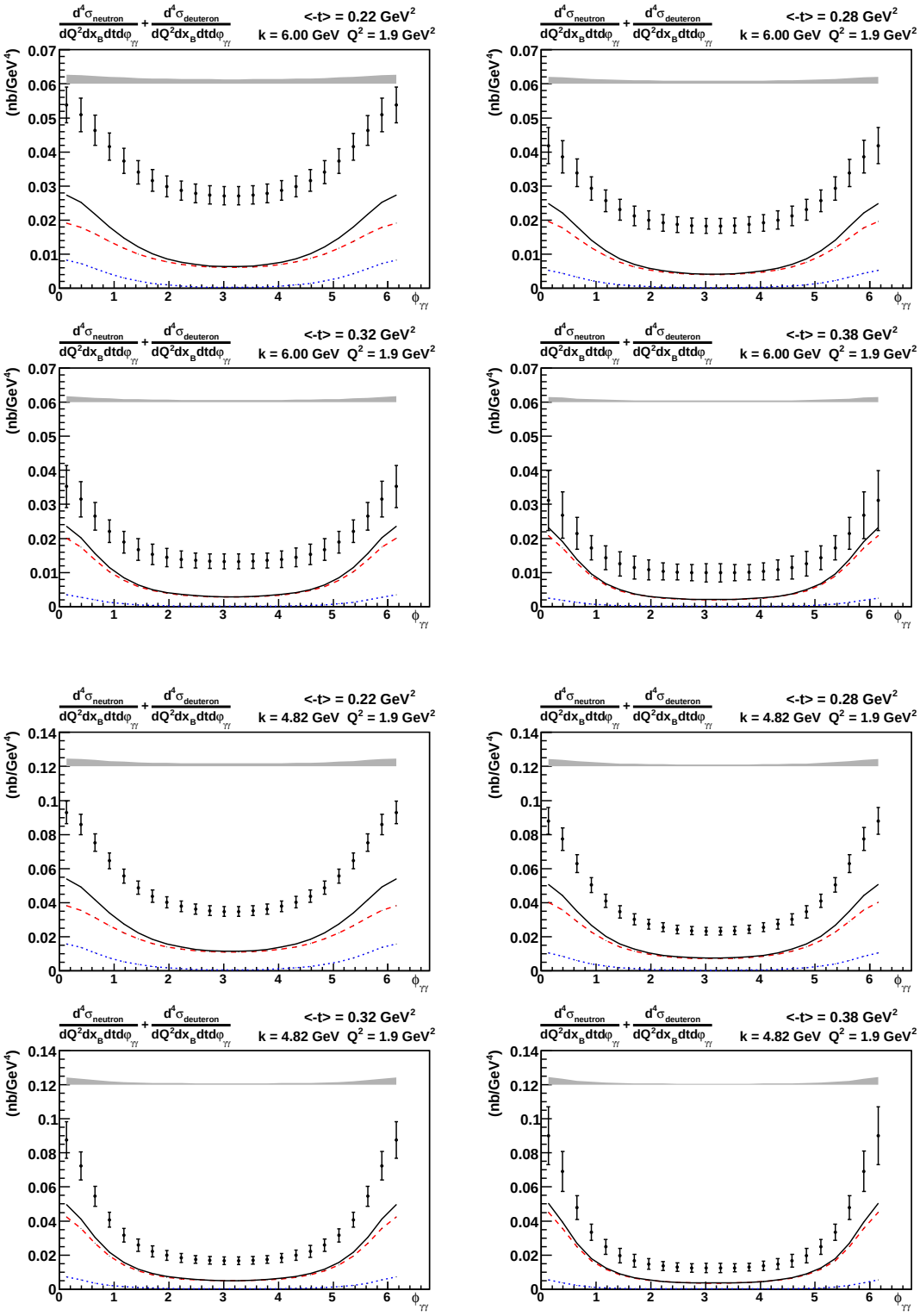

FIG. 17: Projected results and statistical errors of the unpolarized cross sections sum of the photon electroproduction on the neutron (incoherent) and the deuteron (coherent). Shaded bands represent the expected 5% systematic error. The projected results are displayed as a function of $\phi_{\gamma\gamma}$ and t for the requested beam energies 6.0 GeV (top) and 4.82 GeV (bottom). Dashed-dotted (blue) line shows the contribution of the BH on the deuteron; Dashed (red) line shows the BH on the neutron; Solid line is the total BH contribution to the cross section.

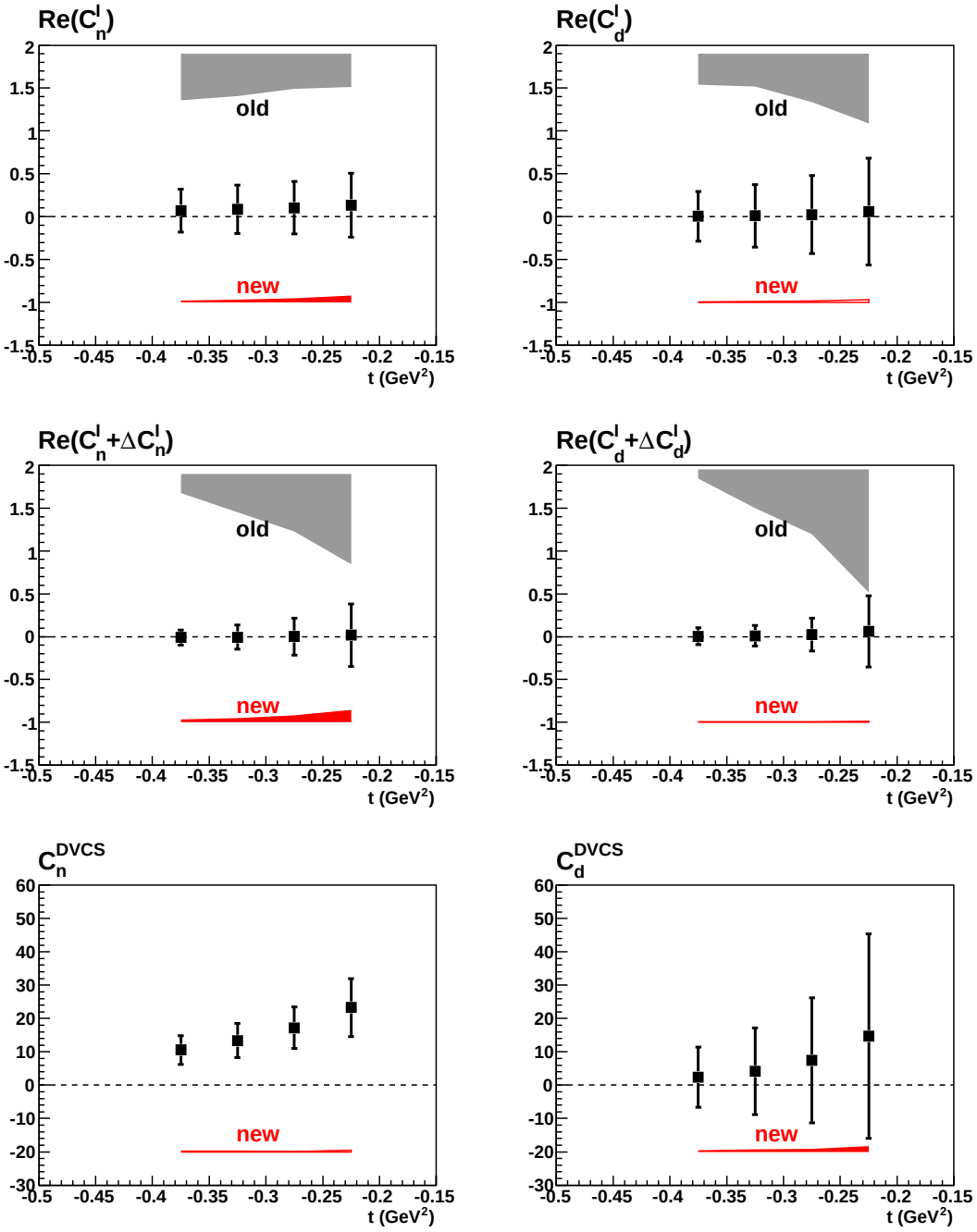

FIG. 18: Expected results and statistical errors of the extracted coefficients for n-DVCS (left) and d-DVCS (right). Systematic errors are indicated by the bottom red bands assuming a 5% total systematic uncertainty on the number of counts. For comparison, E03-106 systematic errors are indicated by the top shaded bands. The determination of E03-106 systematic errors for $\mathcal{C}_{n,d}^{DVCS}$ is impossible with a single beam energy.

IX. SUMMARY

We have learned from the previous neutron experiment that various exciting results are close at hand. We have learned also how to access these results with a few upgrades of the experimental setup and data analysis techniques. The proposed experiment offers the possibility of a better knowledge of the partonic structure of the nucleon through three different approaches :

- The determination of the different contributions of unpolarized cross sections of n-DVCS. That will allow access to combinations of GPD integrals which are complementary to the ones provided by proton experiments.

- The determination of the different contributions of unpolarized cross sections of d-DVCS. The study of d-DVCS process can reveal new nuclear effects and can be linked, within particular models, to nucleon GPDs.

- The determination of deeply virtual π^0 cross sections off the neutron and the evaluation of the longitudinal contributions. This measurement may be linked to GPDs and is complementary to proton measurements.

We request an additional 400 hours beam time to record data with a deuterium target during the future E07-007 experiment. All required detectors and DAQ systems are already planned for E07-007. Apart from the previous E03-106, no other approved DVCS experiments at JLab are dedicated to the neutron or nuclear DVCS. This will be the first measurement of unpolarized n- and d-DVCS cross sections. We believe that performing this experiment will also help to plan and design the future and longer experiments for the upcoming 12 GeV experimental program.

REFERENCES

[1] D. Mueller, D. Robaschik, B. Geyer, F. M. Dittes, and J. Horejsi, Fortschr. Phys. **42**, 101 (1994), hep-ph/9812448.

[2] A. V. Radyushkin, Phys. Rev. **D56**, 5524 (1997), hep-ph/9704207.

[3] X.-D. Ji, Phys. Rev. Lett. **78**, 610 (1997), hep-ph/9603249.

[4] A. Aktas et al. (H1), Eur. Phys. J. **C44**, 1 (2005), hep-ex/0505061.

[5] C. Adloff et al. (H1), Phys. Lett. B **517**, 47 (2001), hep-ex/0107005.

[6] S. Chekanov et al. (ZEUS), Phys. Lett. **B573**, 46 (2003), hep-ex/0305028.

[7] A. Airapetian et al. (HERMES), Phys. Rev. Lett. **87**, 182001 (2001), hep-ex/0106068.

[8] F. Ellinghaus (HERMES), Nucl. Phys. **A711**, 171 (2002), hep-ex/0207029.

[9] A. Airapetian et al. (HERMES), Phys. Rev. **D75**, 011103 (2007), hep-ex/0605108.

[10] S. Stepanyan et al. (CLAS), Phys. Rev. Lett. **87**, 182002 (2001), hep-ex/0107043.

[11] F. X. Girod, R. A. Niyazov, and f. t. C. collaboration (2007), arXiv:0711.4805 [hep-ph].

[12] S. Chen et al. (CLAS), Phys. Rev. Lett. **97**, 072002 (2006), hep-ex/0605012.

[13] C. Muñoz Camacho et al. (Jefferson Lab Hall A), Phys. Rev. Lett. **97**, 262002 (2006), nucl-ex/0607029.

[14] L.L. Frankfurt, P.V. Pobylista, M.V. Polyakov and M. Strikman, Phys. Rev. **D60**, 014010 (1999).

[15] E.R. Berger, F. Cano, M. Diehl and B. Pire, Phys. Rev. Lett. **87**, 142302 (2001).

[16] A. Kirchner and D. Mueller, Eur. Phys. J. **C32**, 347 (2004).

[17] F. Cano and B. Pire, Eur. Phys. J. **A19**, 423 (2004).

[18] M. Mazouz et al. (Jefferson Lab Hall A), Phys. Rev. Lett. **99**, 242501 (2007), nucl-ex/0709.0450.

[19] C. Muñoz Camacho, P.Y. Bertin, C.E. Hyde and J. Roche (spokespersons), E07-007 JLab experiment proposal (2006).

[20] A. V. Belitsky, D. Mueller, and A. Kirchner, Nucl. Phys. **B629**, 323 (2002), hep-ph/0112108.

[21] M. Vanderhaeghen, P. A. M. Guichon, and M. Guidal, Phys. Rev. **D60**, 094017 (1999), hep-ph/9905372.

[22] K. Goeke, M. V. Polyakov, and M. Vanderhaeghen, Prog. Part. Nucl. Phys. **47**, 401 (2001),

hep-ph/0106012.

[23] M. I. Eides, L. L. Frankfurt, and M. I. Strikman, Phys. Rev. **D59**, 114025 (1999), hep-ph/9809277.

[24] M. Vanderhaeghen, J. M. Friedrich, D. Lhuillier, D. Marchand, L. Van Hoorebeke, and J. Van de Wiele, Phys. Rev. **C62**, 025501 (2000), hep-ph/0001100.